Mechanics of Materials 184 (2023) 104691

Contents lists available at ScienceDirect

Mechanics of Materials

journal homepage: www.elsevier.com/locate/mecmat

Research paper

Non-invariant elastic moduli of bi-level architected lattice materials through programmed domain discontinuity

P. Sinha [a], M.G. Walker [b], T. Mukhopadhyay [c,*]

[a] Department of Aerospace Engineering, Indian Institute of Technology Kanpur, Kanpur, India
[b] Department of Civil and Environmental Engineering, University of Surrey, Surrey, UK
[c] Faculty of Engineering and Physical Sciences, University of Southampton, Southampton, UK

ARTICLE INFO

Keywords:
Programmed domain discontinuity
Non-invariant elastic moduli
Bi-level architected materials
Lattice materials
In-plane elastic moduli
Programmable auxeticity

ABSTRACT

Effective elastic moduli of lattice-based materials are one of the most crucial parameters for the adoption of such artificial microstructures in advanced mechanical and structural systems as per various application-specific demands. In conventional naturally occurring materials, these elastic moduli remain invariant under tensile and compressive normal modes or clock-wise and anti-clock-wise shear modes. Here we introduce programmed domain discontinuities in the cell walls of the unit-cells of lattice metamaterials involving a bi-level microstructural design to achieve non-invariant elastic moduli under tensile and compressive normal modes or clock-wise and anti-clock-wise shear modes. More interestingly, such non-invariance can be realized in the linear small deformation regime and the elastic moduli can be tailored to have higher or lower value in any mode compared to the other depending on the placement and intensity of the discontinuities in a programmable paradigm. We have derived an efficient analytical framework for the effective elastic moduli of lattice materials taking into account the influence of domain discontinuity. The axial and shear deformations at the beam level are considered along with bending deformation in the proposed analytical expressions. The numerical results ascertain that the domain discontinuities, in conjunction with unit cell level geometric parameters, can impact the effective elastic constants significantly under different modes of far-field stresses. It is further revealed that the degree of auxeticity of such lattices can be programmed to have target values (including non-invariance under different modes of deformation) as a function of the intensity and location of domain discontinuity when axial and shear deformations are included at the beam level. Realization of the unusual non-invariant elastic moduli of bi-level architected lattice materials would lead to a range of technologically demanding niche applications where one mode of deformation requires more or less force to deform compared to the opposite mode. Besides being able to perform as a load-bearing component, the proposed metamaterial can be used as an integrated sensor for measuring the level of stress or strain in structures.

1. Introduction

Artificially engineered lattice-based materials, a class of mechanical metamaterials, exhibit mechanical properties which are not found in conventional structural materials directly obtained from nature (Sinha and Mukhopadhyay, 2023). Their microstructural design can result in unprecedented characteristics such as negative mass density, negative elastic moduli, auxeticity, ultra property characteristics like specific strength and stiffness, lightweight features, meta-fluid properties, tunable constitutive relations, active and programmable properties etc. Mukhopadhyay et al. (2020a), Kolken and Zadpoor (2017), Mukhopadhyay et al. (2019), Fleck et al. (2010), Lai et al. (2011), Karlicic et al. (2021), Cummer et al. (2016), Singh et al. (2022) and Isanaka et al. (2022). They have attracted the scientific community due to their properties that span across different ranges catering to application-specific multi-functional demands of the modern industry.

Periodic structural forms and lattices are available in naturally occurring systems as well as engineered mechanical systems in plenty across the length scales (Ding et al., 2019; Mukhopadhyay and Adhikari, 2017; Gibson and Ashby, 1999). Sandwich structures exploit the lightweight property along with high specific stiffness of honeycomb lattices as cores making them attractive for different mechanical and structural systems (Yongquiang and Zhiquiang, 2008; Mukhopadhyay and Adhikari, 2016b; Zenkert, 1995). Apart from being found across macro and micro scales, the lattice

* Corresponding author.
E-mail address: t.mukhopadhyay@soton.ac.uk (T. Mukhopadhyay).

https://doi.org/10.1016/j.mechmat.2023.104691
Received 5 January 2023; Received in revised form 26 April 2023; Accepted 17 May 2023
Available online 20 June 2023

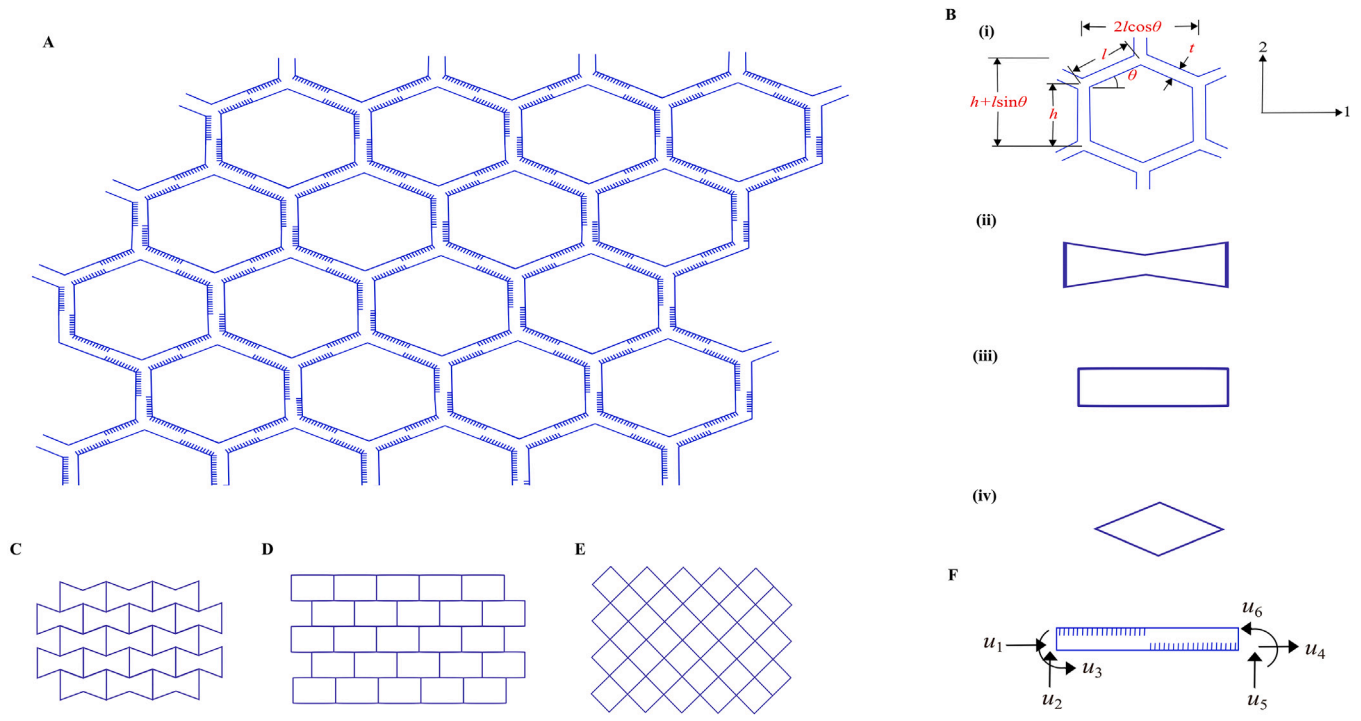

Fig. 1. Bi-level unit cell based approach for analyzing non-invariant lattices. (A) A typical regular honeycomb lattice with programmed domain discontinuity (zero-thickness cuts partially across the depth). **(B)** Unit cells that can represent the entire honeycomb lattice. **(i)** Non-auxetic hexagonal unit cell. **(ii)** Auxetic hexagonal unit cell. **(iii)** Rectangular unit cell. **(iiv)** Rhombic unit cell. **(C–E)** Structural derivatives of a hexagonal lattice that can be obtained by considering the geometric parameters appropriately. For example, the re-entrant auxetic structure (with negative Poisson's ratio), rectangular lattice structure and rhombic lattice structure can be obtained by considering θ as negative, θ as zero and h as zero, respectively. **(F)** Degrees of freedom of a single cell wall with cuts, considering it as a beam element. The lattice is formed from periodic repetition of these beams. Here, a bottom-up methodology is adopted for analyzing the effective elastic moduli of lattice materials. We have taken into account the deformation mechanics of the beam-like members at local-level in the analysis considering bending, axial and shear deformation in conjunction with the effect of the cuts introduced. Then we analyze a unit cell which is made-up of beam-like members to derive the analytical formulations of the five in-plane elastic moduli. At this stage, we have considered the effect of geometry of the unit cells. The elastic moduli thus derived following a unit cell based approach could subsequently be utilized in the design of different engineering structures.

structures are also available in nano-scale (Mukhopadhyay et al., 2017). Normally a unit cell (Gibson and Ashby, 1999) or representative volume element (Omairey et al., 2019) based approach is adopted to evaluate the effective mechanical properties of such periodic structures. Based on unit cell approach, anisotropy and elasticity tailoring in lattices made up of constituting members of multiple materials is presented in a recent study (Mukhopadhyay et al., 2020b, 2023) that essentially stretches the design sphere when compared to uni-material lattices, where geometry of microstructure is the most influential parameter. More lately, the Young's moduli are found to be actively modulated by varying the voltage in peizo-electric lattice materials (Singh et al., 2020). The irregularities in lattice materials due to manufacturing has been looked into by considering voronoi honeycombs (Li et al., 2005; Zhu et al., 2001, 2006) and controlled random distortion of the periodic geometry (Mukhopadhyay and Adhikari, 2016a, 2017). The effect of intrinsic pre-existing stresses have been studied for honeycombs that can essentially be attributed to manufacturing irregularities or additional design parameter for novel material innovation (Sinha and Mukhopadhyay, 2022). A study on the geometric non-linear response of lattice materials to obtain their large-strain elastic response has been reported (ElNady et al., 2016). Exploiting the periodicity of lattice structures, the effective elastic properties of 2D lattices have been computed using mechanics based codes (Karathanasopoulos et al., 2020). A large volume of works in the field of architected materials include the evaluation of elastic properties using homogenized response of lattice materials (Dos Reis and Ganghoffer, 2014; El Nady et al., 2017; Rahali et al., 2017; Dos Reis and Ganghoffer, 2012a,b; Karathanasopoulos et al., 2018). Some of the other critical recent developments concerning elastic properties of honeycomb lattice metamaterials involve nonlinear anti-curvature lattices (Ghuku and Mukhopadhyay, 2022; Prajwal et al., 2022; Ghuku and Mukhopadhyay, 2022), chiral, anti-chiral, hierarchical (Mousanezhad et al., 2016), bi-level micro-topology architected lattices (Kundu et al., 2022) and 3D connected double loop (3DCDL) lattices (Mukhopadhyay and Kundu, 2022).

A careful review of the recent literature on honeycomb lattices reveals that several studies have been reported to modulate the effective elastic properties primarily depending on the unit cell geometry. In this paper we focus on a relatively new approach of bi-level designs, wherein the effective lattice-level properties are functions of unit cell geometry as well as beam-level architecture. Based on such bi-level design paradigm we aim to propose novel metamaterials with non-invariant (i.e. not same) elastic moduli under different modes of deformation within the linear elastic regime (refer to Fig. 1). In conventional materials, the elastic moduli under tension and compression modes or clockwise and anti-clockwise shear modes are normally invariant (i.e. same) within the linear elastic regime. To modify this behavior, one straightforward architecture could be to introduce discontinuities (zero-width or near-zero width cuts) as shown in Fig. 2(A, B). It can be realized that the stress required to deform such structures under tension would be lesser than that under compression because of the fact that different cross-sectional areas participate in bearing the applied load for the two different modes of deformation. If a metamaterial is designed based on this concept by adopting such architecture at the microscale, it is possible to have non-invariant Young's modulus under tension and compression. However, the tensile Young's modulus will always be lesser than that in the compressive mode for this particular architecture. In this paper, we exploit the idea of domain discontinuity (zero-width or near-zero width cuts) to extend it further in the framework of lattice based bi-level architectures (refer to Fig. 1) to achieve non-invariant effective elastic moduli under normal and shear modes (within the linear elastic regime), where any one of the modes (tension and compression or clock-wise and anti-clockwise) can have higher or lower elastic moduli compared to the opposite mode. The extent of difference between the

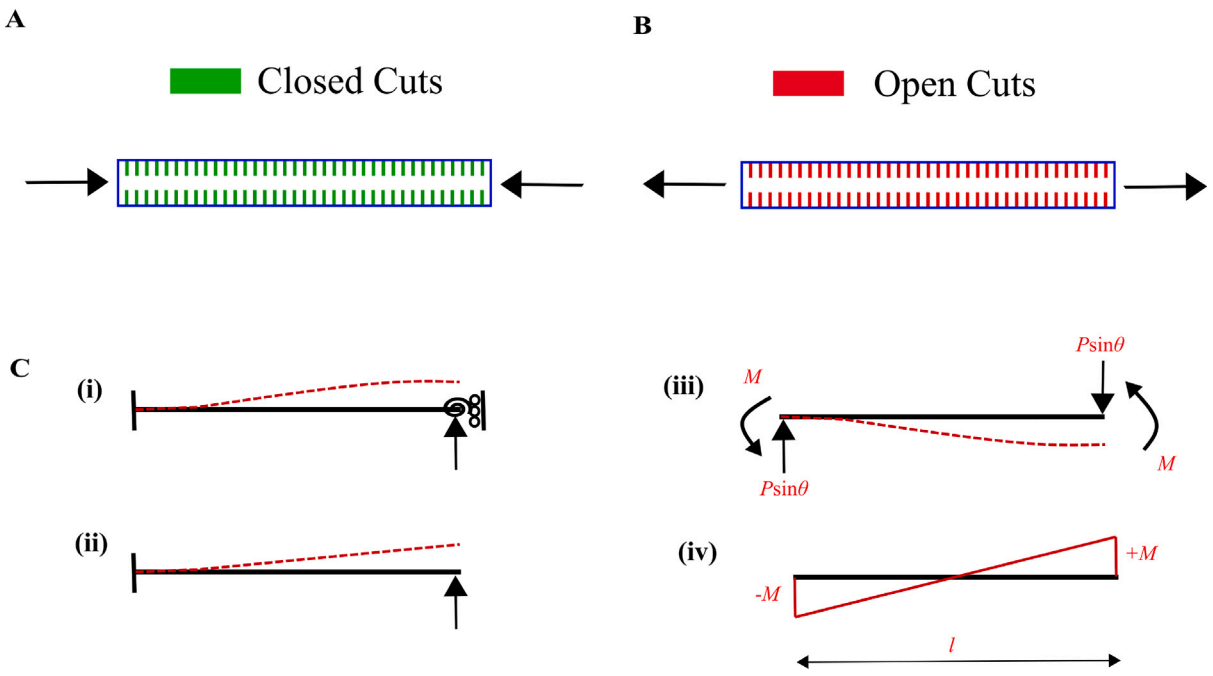

Fig. 2. A typical beam with domain discontinuity. **(A)** Behavior of a simple beam with cuts in compression. **(B)** Behavior of a simple beam with cuts in tension. **(C)** Beams with three different boundary conditions. **(i)** Beam with one end clamped and no rotation allowed at the other. **(ii)** Beam with one end clamped and other free. **(iii)** Free body diagram of the slant member of a hexagonal unit cell considered for derivation of elastic moduli (refer Fig. 3). **(iv)** Bending moment diagram of the slant member of unit cell, denoting that it acts similar to two cantilever beams of lengths $l/2$ joined at the center (note that bending moment is zero at the center).

two opposite modes (i.e. degree of non- invariance; expressed as a ratio later in this paper) and which of the modes provides higher elastic moduli would depend on the placement of the discontinuities as well as the depth of the cuts. Besides investigating the effective Young's moduli and shear modulus, we also aim to investigate the non-invariance in in-plane Poisson's ratios under tensile and compressive modes.

In the current work, we will first utilize the Euler–Bernoulli beam theory to derive the analytical formulations of the effective elastic moduli for the lattice-based non-invariant metamaterials taking into account the bending deflections of the beam-like members. Then we will extend the framework to account for the effect of axial deflection and shear deformation (Timoshenko beam theory) at the beam-level for a more generalized and accurate analysis. In this article, we deal essentially with lattices of hexagonal shape (refer to Fig. 1(A)) with non-auxetic and auxetic configurations along with their derivatives such as rhombic and rectangular lattices (refer to Fig. 1(B–E)). Note that hexagonal lattices and their derivatives are chosen here as they are primarily bending dominated and the non-invariant properties with the flexibility of having higher values in either tensile or compressive modes (and clockwise or anti-clockwise modes) are achievable, which may not necessarily be the case in stretching dominated lattices. This article is, henceforth, structured as follows, Section 2: mechanics-based derivation of the formulations of non-invariant elastic moduli of lattices with domain discontinuities, Section 3: numerical results taking into account different lattice geometries and configurations, Section 4: conclusion and prospective impact of the current work.

2. Analytical derivation for effective elastic moduli of non-invariant lattice metamaterials

We have followed a bi-level bottom-up approach to calculate the elastic moduli based on the basic definitions by obtaining the stress and corresponding strain components. Since the lattices are periodic structures, a unit cell can be analyzed with periodic boundary conditions to evaluate the effective homogenized properties of the entire lattice. The global stress field is uniform in a periodic structure and it can be converted to point loads at the joints of the unit cells locally based on the dimensions and periodicity of the unit cells. Further, since each of the unit cells consists of a collection of beams, the total deformation and strain of the unit cell are derived based on the combined effect of these beam deformations. However, the loading and boundary conditions of these beams need to be carefully imposed to conform the unit cell level periodicity and global uniform stress field. In such unit cell based analyses, the implicit assumption is that there is a large number of cells (normally more than 21×21 cells, approximately) so that the boundary effects become negligible. While the unit cell level structural properties such as $h/l, t/l, \theta, \alpha$ define the effective elastic moduli, for a particular geometry of the unit cell (i.e. a set of these values), the number of unit cells will not have any effect on the homogenized effective elastic moduli beyond the converged number of cells as mentioned above.

Here, we would derive the five independent in-plane elastic constants of hexagonal honeycomb lattices with domain discontinuity (zero-width or near-zero width cuts) by considering a unit cell with beam-like members as shown in Fig. 1(A, B(i) and F). For that purpose, we analyze the local-level deformation behavior of the beam members as shown in Fig. 1(F), which are then used in the derivation of analytical formulations of the elastic constants of the hexagonal lattice through a unit cell based approach. The effective elastic constants thus derived following a unit cell framework is representative of overall mechanical characteristics of the lattice material (refer to Fig. 1(A)) that could subsequently be adopted for further structural designing.

At the beam level, we define E, the Young's modulus of the constituting beam-like members and at the global level, the in-plane elastic constants (E_1, E_2, ν_{12}, ν_{21} and G_{12}) are derived for the entire lattice. Thus the lattice-level effective elastic moduli are functions of both E as well as the beam and unit-cell level architectures. This allows us to have different elastic constants based on different geometric parameters (beam and unit cell

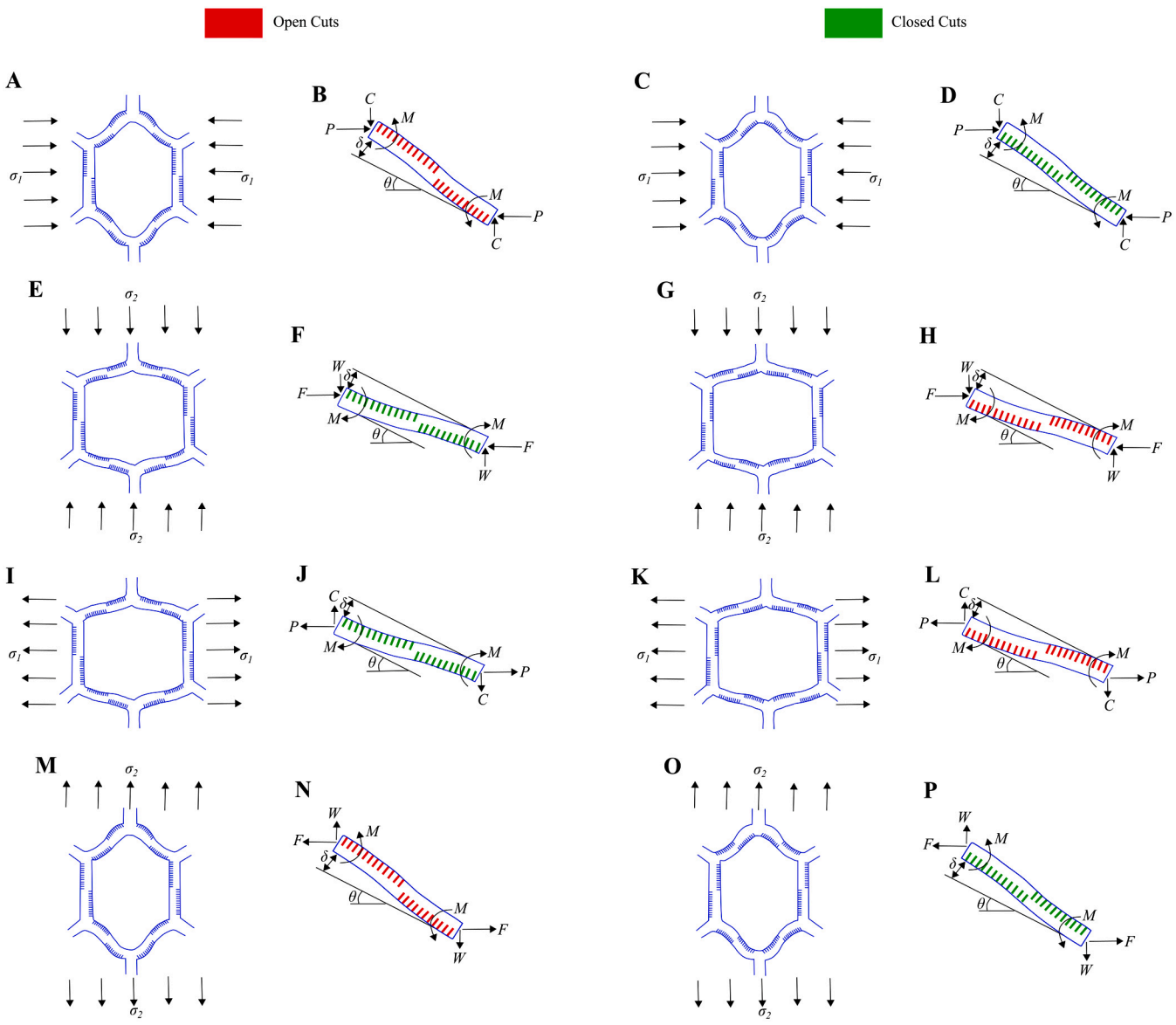

Fig. 3. Mechanics of non-invariant honeycombs under different normal far-field stress conditions. Based on the placement of domain discontinuity, we propose two different configurations here as shown in the two columns of subfigures (Configuration 1 in the left column and Configuration 2 in the right column). **(A, C)** Deformation behavior of a honeycomb subjected to uniform compressive stress field σ_1 applied in the direction-1, for Configuration 1 and Configuration 2, respectively. **(B, D)** Bending deformation of the slant member of the honeycomb subjected to compressive stress field σ_1, for Configuration 1 and Configuration 2, respectively. The longitudinal Young's modulus E_1 and the Poisson's ratio ν_{12} are derived from this configuration. **(E, G)** Deformation behavior of a honeycomb subjected to uniform compressive stress field σ_2 applied in the direction-2, for Configuration 1 and Configuration 2, respectively. **(F, H)** Bending deformation of a slant member of the honeycomb subjected to compressive stress field σ_2, for Configuration 1 and Configuration 2, respectively. The derivations of the transverse Young's modulus E_2 and the Poisson's ratio ν_{21} are carried out using this configuration. **(I, K)** Deformation mechanics of a honeycomb under the uniform tensile stress field σ_1 applied in the direction-1, for Configuration 1 and Configuration 2, respectively. **(J, L)** Bending deformation of a slant member of the honeycomb subjected to tensile stress field σ_1, for Configuration 1 and Configuration 2, respectively. **(M, O)** Deformation mechanics of a honeycomb under the uniform tensile stress field σ_2 applied in the direction-2, for Configuration 1 and Configuration 2, respectively. **(N, P)** Bending deformation of a slant member of the honeycomb subjected to tensile stress field σ_2, for Configuration 1 and Configuration 2, respectively. The open cuts are shown using red color and the closed ones using green color. (For interpretation of the references to color in this figure legend, the reader is referred to the web version of this article.)

level architectures), while keeping the intrinsic material unchanged. In this article, the focus is on beam-level architecture in the form of domain discontinuity (zero-width or near-zero width cuts) that leads to the non-invariant elastic behavior. The global lattice-level non-invariant behavior depends on the placement of cuts, based on which we propose two different configurations here.

As shown in Fig. 1(A), we place the cuts in two halves of the constituting beams in two opposite faces. The typical deformed shapes of the honeycomb unit cells under different modes of normal and shear stresses are shown in Figs. 3 and 4, wherein it becomes evident that the cuts in both halves of the beams will either open or close in the opposite modes of normal and shear deformations. This leads to a non-invariant behavior under tension and compression, or clockwise and anti-clockwise shear. We propose two configurations of beam-level architecture: Figs. 3(A, E, I and M) show Configuration 1 and Figs. 3(C, G, K and O) show the Configuration 2. Depending on whether the cuts open or close, the elastic moduli under one mode will be lower or higher compared to the opposite mode, respectively. For example, Young's modulus for direction 1 corresponding to the Configuration 1 will have higher value in tensile mode compared to the compressive mode, while an opposite behavior would be realized for the Configuration 2.

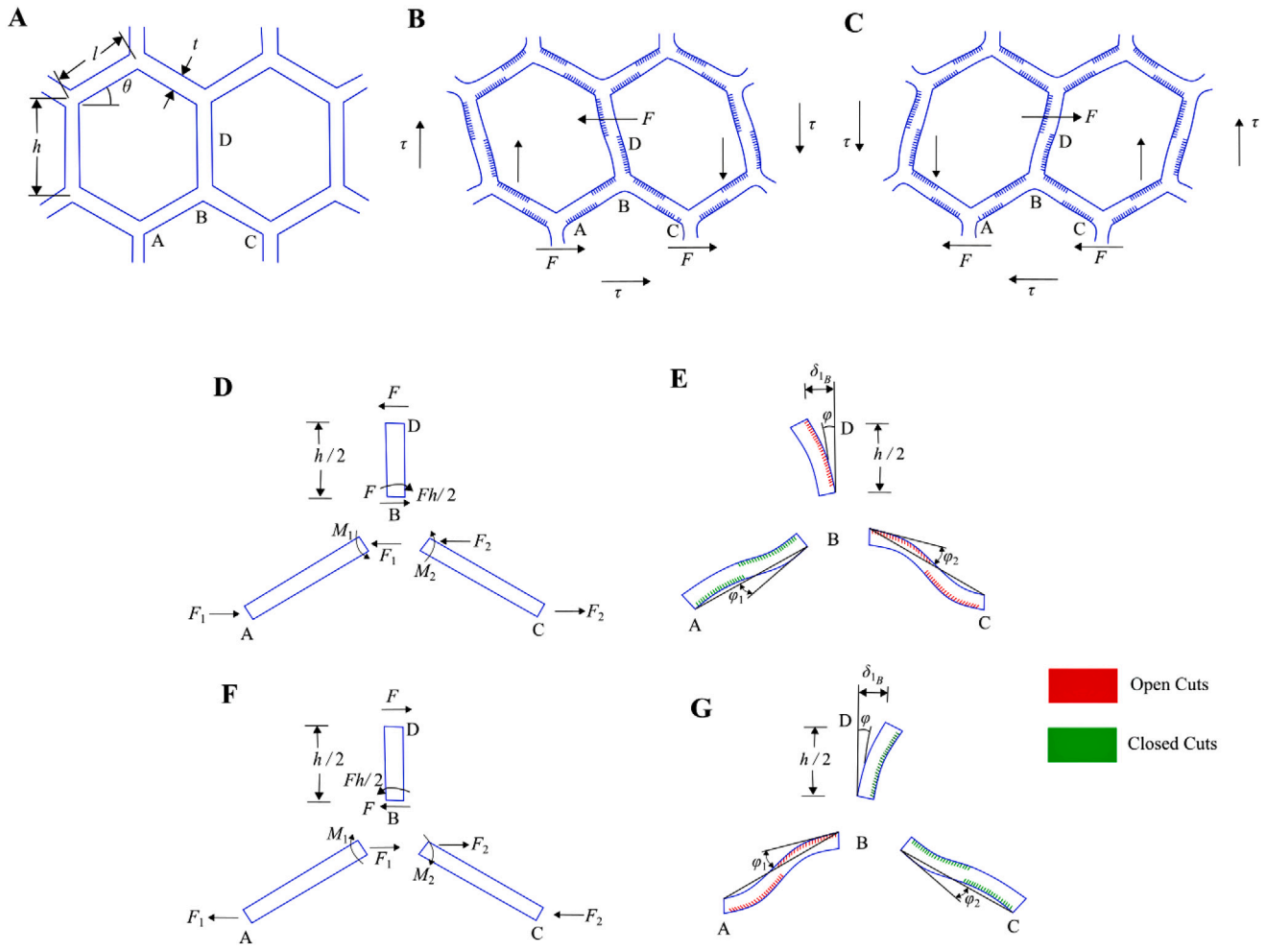

Fig. 4. Mechanics of non-invariant honeycombs under different shear stress conditions. (A) Typical shapes of undeformed honeycomb lattice unit cells for evaluating in-plane shear modulus. **(B)** Deformation behavior of a honeycomb subjected to the anti-clockwise shear stress field τ. **(C)** Deformation behavior of a honeycomb subjected to clockwise shear stress field τ. **(D)** Forces and moments acting on the honeycomb members under the anti-clockwise shear stress field τ. **(E)** Displacements and rotations of the honeycomb members subjected to anti-clockwise shear stress field τ. We would use this configuration to derive the shear modulus G_{12}^{-}. Here the cuts of the members BD and BC open as they are in tension, while those of the member AB close as they are in compression. **(F)** Forces and moments acting on the honeycomb members under clockwise shear stress field τ. **(G)** Displacements and rotations of the honeycomb members subjected to clockwise shear stress field τ. We would use this configuration to derive the shear modulus G_{12}^{+}. Here the cuts of the members BD and BC close as they are in compression, while those of the member AB open as they are in tension. The open cuts are shown using red color and the closed ones using green color. Note that this figures are used for deriving the shear moduli considering beam-level bending deformations. (For interpretation of the references to color in this figure legend, the reader is referred to the web version of this article.)

2.1. In-plane elastic properties of Configuration 1

2.1.1. In-plane elastic moduli considering only beam-level bending deformation

2.1.1.1. Longitudinal Young's modulus E_1. To obtain the analytical formulation of longitudinal Young's modulus, we consider that the unit cell is subjected to a uniform compressive stress σ_1 in the longitudinal direction. This stress gives rise to force P at the ends of the constituting beam member (refer to Fig. 3(A–B)). The force P that acts on the joints of a member of the unit cell, in the direction of the applied stress, σ_1 is given as

$$P = \sigma_1 b(h + l\sin\theta) \tag{1}$$

Fig. 3(B) shows the deformed shape of the slant member of the unit cell, with δ depicting the transverse deformation of the inclined member. When in compression due to the application of σ_1, the cuts that are on the convex side of the deformed member open up. Let the depth of cuts be αt, where α (where $0 \leq \alpha < 1$) is a parameter defining intensity of the cuts and t is the thickness of the cell walls. When the value of α is 0, it means that there is no cut and it acts like conventional beams. This is also the case of closing cuts under a certain mode of lattice-level deformation. When the value of α tends to 1, it corresponds to the case of a discontinuous beam, leading to lattices with zero elastic moduli (or in other words, not a feasible microstructural configuration). Thus the value of α needs to be less than 1. As the value of α increases from 0 towards 1, the lattice becomes softer and the elastic moduli reduce under the opening mode of beam deformations. In the present work, there is an implicit assumption that the lattice does not fail due to material failure, buckling, or plasticity. We deal with the small deformation regime where the linear elasticity theory is valid. However, under large deformation, there is a scope for defining the upper limit of α based on beam-level failure criteria. In such cases, beam length-wise programmed gradation in α can further be introduced to enhance the failure strength. The consideration of failure strength is beyond the scope of this paper and we keep it for future studies. In Eq. (1), b represents the width of the rectangular beam cross-section. It is

a dimension in the direction perpendicular to the 2D plane of the lattice. We get the corresponding second moment of inertia, $I = \frac{b[t(1-\alpha)]^3}{12}$ when the cuts open. However, we have $I = \frac{bt^3}{12}$, when the cuts close. For all the lattice-level analyses carried out in this paper under normal and shear stresses can be performed by considering two different boundary conditions: (1) one end clamped and the other end rotationally restrained (translation allowed) with transverse point load applied to the rotationally restrained end, (2) a cantilever beam with transverse point load applied to the fixed end. The boundary conditions and deflection profile for the first case is shown in Fig. 2(C)(i) and that for a cantilever beam is shown in Fig. 2(C)(ii). Noting that the bending moment at the midpoint of a slant beam is zero (refer to Fig. 2(C)(iii) and (iv)), we realize that the transverse deflection of the end point for a full-length beam with the first boundary condition can also be found out by analyzing a half-length beam with cantilever boundary condition. Thus, the deflection δ can be expressed as

$$\begin{aligned}\delta &= 2 \times \frac{P \sin\theta\,(l/2)^3}{3EI} \\ &= \left(\frac{l}{t}\right)^3 \frac{P \sin\theta}{bE\,(1-\alpha)^3}\end{aligned} \tag{2}$$

The moment M (given by $M = Pl\sin\theta/2$), shown in Fig. 3(B), has a much higher value than the couple M_t (given by $M_t = P\cos\theta\alpha t$) arising due the force P, and thus we ignore the effect of the couple with the assumption $M \gg M_t$, which leads to

$$\tan\theta \gg 2\alpha\left(\frac{t}{l}\right) \tag{3}$$

The above relation is strictly valid for thin to moderately thick cell wall of honeycombs. Total deflection along σ_1 (i.e. direction -1) is $\delta_1 = \delta\sin\theta$. Strain along direction of σ_1 is, therefore, given as

$$\begin{aligned}\varepsilon_1 &= \frac{\delta_1}{l\cos\theta} \\ &= \frac{Pl^2\sin^2\theta}{bEt^3\,(1-\alpha)^3\cos\theta} \\ &= \left(\frac{l}{t}\right)^3 \frac{\sigma_1\left(\frac{h}{l}+\sin\theta\right)\sin^2\theta}{E\,(1-\alpha)^3\cos\theta}\end{aligned} \tag{4}$$

Now the Young's modulus along direction-1, under the application of compressive stress σ_1 can be given by

$$\begin{aligned}E_1^C &= \frac{\sigma_1}{\varepsilon_1} \\ &= \left(\frac{t}{l}\right)^3 \frac{E\,(1-\alpha)^3\cos\theta}{\left(\frac{h}{l}+\sin\theta\right)\sin^2\theta}\end{aligned} \tag{5}$$

Similarly, let us consider tensile stress σ_1 be applied to the unit cell for the derivation of longitudinal Young's Modulus. The cuts get closed in this case (unlike under the compressive far-field stress) as they now are in concave regions of the deformed member (refer Fig. 3(E–F)). The derivation of E_1 under application of uniform tensile stress is similar to as done above, except that in this case $\alpha = 0$. So the longitudinal Young's modulus under tensile stress σ_1, is given by

$$E_1^T = \left(\frac{t}{l}\right)^3 \frac{E\cos\theta}{\left(\frac{h}{l}+\sin\theta\right)\sin^2\theta} \tag{6}$$

The ratio of longitudinal Young's modulus under application of tensile stress to that under application of compressive stress is obtained by using the expressions (6) and (5)

$$\frac{E_1^T}{E_1^C} = \frac{1}{(1-\alpha)^3} \tag{7}$$

This ratio defines the degree of non-invariance of longitudinal Young's moduli under tension and compression, which depends on α.

2.1.1.2. Poisson's ratio ν_{12}. To obtain the Poisson's ratio ν_{12}, we require the strain in transverse direction (i.e., direction-2), due to the compressive stress σ_1, as shown in Fig. 3(A). From Eq. (2), we obtain the total deflection in transverse direction (δ_2), which is given as

$$\begin{aligned}-\delta_2 &= \delta\cos\theta \\ &= \left(\frac{l}{t}\right)^3 \frac{P\sin\theta\cos\theta}{bE\,(1-\alpha)^3}\end{aligned} \tag{8}$$

Total strain in the transverse direction is given as

$$\begin{aligned}-\varepsilon_2 &= \frac{\delta_2}{h + l\sin\theta} \\ &= \left(\frac{l}{t}\right)^3 \frac{P\sin\theta\cos\theta}{bE\,(h+l\sin\theta)\,(1-\alpha)^3}\end{aligned} \tag{9}$$

From the Eqs. (4) and (9), the Poisson's ratio ν_{12} is expressed as

$$\nu_{12} = -\frac{\varepsilon_2}{\varepsilon_1} = \frac{\cos^2\theta}{\left(\frac{h}{l}+\sin\theta\right)\sin\theta} \tag{10}$$

Since Eq. (10) is the ratio of strains in two directions, it is identical under either compressive or tensile stress (i.e. degree of non-invariance for ν_{12} is 1).

2.1.1.3. Transverse Young's modulus E_2. To obtain transverse Young's modulus E_2, we consider that a uniform far-field compressive stress σ_2 is applied on the unit cell in direction-2. From the free-body diagram of the constituting beam members of the unit cell, we find that the applied stress gives rise to a vertical force W. The magnitude of W is given by (refer to Fig. 3(C–D))

$$W = \sigma_2 bl \cos\theta \tag{11}$$

When in compression due to the application of σ_2, the cuts fall on the concave side of the deformed member and thus close. Here, the second moment of inertia is $I = \frac{bt^3}{12}$. The bending moment at the centre of the slant members is zero, i.e., it acts similar to two cantilever beams joined at the centre. Thus, the deflection δ can be expressed as

$$\begin{aligned}\delta &= 2 \times \frac{W \cos\theta\,(l/2)^3}{3EI} \\ &= \left(\frac{l}{t}\right)^3 \frac{W\cos\theta}{bE}\end{aligned} \tag{12}$$

Total deflection along direction-2 is $\delta_2 = \delta\cos\theta$. Note that the assumption as given in Eq. (3) holds here as well. Strain along direction of σ_2 is, therefore, given as

$$\begin{aligned}\varepsilon_2 &= \frac{\delta_2}{h + l\sin\theta} \\ &= \left(\frac{l}{t}\right)^3 \frac{W\cos^2\theta}{bE\,(h + l\sin\theta)} \\ &= \left(\frac{l}{t}\right)^3 \frac{\sigma_2 \cos^3\theta}{E\left(\frac{h}{l} + \sin\theta\right)}\end{aligned} \tag{13}$$

Thus, the transverse Young's modulus in direction-2, under compressive stress σ_2, is expressed as

$$E_2^C = \frac{\sigma_2}{\varepsilon_2} = \left(\frac{t}{l}\right)^3 \frac{E\left(\frac{h}{l} + \sin\theta\right)}{\cos^3\theta} \tag{14}$$

Similarly, let us consider far-field tensile stress σ_2 to be acting on the unit cell in the direction opposite to direction-2 for the derivation of transverse Young's modulus. The cuts open up as they are now in convex regions of the deformed members. The derivation of E_2 under application of uniform tensile stress is similar to as done above, except that in this case $I = \frac{b[t(1-\alpha)]^3}{12}$, where αt is the depth of cuts. Fig. 3(G) shows a uniform tensile stress σ_2 acting on the unit cell. If we consider a beam element of the unit cell, the stress gives rise to a vertical force W, the magnitude of which is expressed as (refer to Fig. 3(H))

$$W = \sigma_2 bl \cos\theta \tag{15}$$

The bending moment at the centre of the member is zero. Thus, the deflection δ can be expressed as

$$\begin{aligned}\delta &= 2 \times \frac{W \cos\theta\,(l/2)^3}{3EI} \\ &= \left(\frac{l}{t}\right)^3 \frac{W\cos\theta}{bE\,(1-\alpha)^3}\end{aligned} \tag{16}$$

Total deflection along direction-2 is $\delta_2 = \delta\cos\theta$. Strain along direction of σ_2 is, therefore, given as

$$\begin{aligned}\varepsilon_2 &= \frac{\delta_2}{h + l\sin\theta} \\ &= \left(\frac{l}{t}\right)^3 \frac{W\cos^2\theta}{bE\,(h + l\sin\theta)\,(1-\alpha)^3} \\ &= \left(\frac{l}{t}\right)^3 \frac{\sigma_2 \cos^3\theta}{E\left(\frac{h}{l} + \sin\theta\right)(1-\alpha)^3}\end{aligned} \tag{17}$$

Therefore, the transverse Young's modulus, under application of tensile stress, can be expressed in closed-form as

$$E_2^T = \left(\frac{t}{l}\right)^3 \frac{E\left(\frac{h}{l} + \sin\theta\right)(1-\alpha)^3}{\cos^3\theta} \tag{18}$$

The ratio of transverse Young's modulus under application of tensile stress to that under application of compressive stress is obtained by using the expressions (18) and (14)

$$\frac{E_2^T}{E_2^C} = (1-\alpha)^3 \tag{19}$$

This ratio defines the degree of non-invariance of transverse Young's moduli under tension and compression, which depends on α.

2.1.1.4. Poisson's ratio ν_{21}. For deriving the Poisson's ratio ν_{21}, we require the strain in longitudinal direction, resulting from the stress σ_2. The magnitude of deformation in longitudinal direction under the stress σ_2 in transverse direction is given by (refer to Fig. 3(C–D))

$$\begin{aligned}\delta_1 &= -\delta\sin\theta \\ &= -\left(\frac{l}{t}\right)^3 \frac{W\sin\theta\cos\theta}{bE\,(1-\alpha)^3}\end{aligned} \tag{20}$$

The strain in longitudinal direction is, thus, given as

$$\varepsilon_1 = \frac{\delta_1}{l\cos\theta} = -\frac{Wl^2\sin\theta}{Ebt^3(1-\alpha)^3} \tag{21}$$

From the Eqs. (17) and (21), we obtain the Poisson's ratio ν_{21}, which is given as

$$\nu_{21} = -\frac{\varepsilon_1}{\varepsilon_2} = \frac{\left(\frac{h}{l}+\sin\theta\right)\sin\theta}{\cos^2\theta} \tag{22}$$

Since Eq. (22) is the ratio of strains in two directions, it is similar for the unit cell under either compressive or tensile stress (i.e. degree of non-invariance for ν_{21} is 1).

2.1.1.5. Shear modulus G_{12}. First we consider the case when far-field shear stress is applied in the anti-clockwise direction. To derive the shear modulus G_{12}, we will consider the member BD, which has the cuts on the right side, that is the convex side of the member (refer Fig. 4(A–B)). We have considered bending deformation of the cell walls and it can be noticed that mid-point of the vertical member, under the impact of far-field shear stress, deforms only in direction-1. Thus, we consider the unit cell as shown in Fig. 4(D–E), where the length of the vertical member is $h/2$ and that of the slant members is l. Between joints A and B, the relative movement is not there due to symmetry.

The shear strain resulting from bending is denoted by γ. There are two components of this strain. First arises from the bending deflection of BD while the second arises due to its deflection caused from the joint rotation of B because of the bending of inclined members. When shear force F (under anti-clockwise far-field shear stress) acts on the member BD, the cuts open up. Along direction-1, the deformation of point D due to bending with respect to point B, considering a member of $h/2$ length, is expressed as

$$\begin{aligned}\eta_d &= \frac{F(h/2)^3}{3EI} \\ &= \frac{Fh^3}{2Ebt^3(1-\alpha)^3}\end{aligned} \tag{23}$$

where F is given as

$$F = 2\tau lb\cos\theta \tag{24}$$

The point B is acted upon by a moment (refer to Fig. 4(D)), which is given as

$$M = \frac{Fh}{2} \tag{25}$$

At this point it may be noted that the moment and forces coming from the vertical member would not be equally distributed to the slant members as their stiffness would be different. Under anti-clockwise far-field stress the cuts in member AB close, while that in member BC open. From the analysis of the slant member AB, value of moment is given as

$$M_1 = \frac{\bar{F}_1 l}{2} \tag{26}$$

Here $\bar{F}_1$ is the transverse end forces at the two ends of the slant members. The slant member deforms as shown in Fig. 4(E). The cuts in AB come under compression and thus close. The deflection of joint B with reference to joint A under the impact of moment M_1 at B, can be expressed as

$$\delta_r = \frac{\bar{F}_1 l^3}{12EI} = \left(\frac{l}{t}\right)^3 \frac{\bar{F}_1}{bE} \tag{27}$$

Using Eq. (26) and Eq. (27), we get

$$\delta_{r_1} = \frac{2M_1 l^2}{Ebt^3} \tag{28}$$

The rotation of the member AB is then given by

$$\varphi_1 = \frac{\delta_{r_1}}{l} = \frac{2M_1 l}{Ebt^3} \tag{29}$$

The rotation of the member BC, due to application of moment M_2, is obtained in a similar way, except that the cuts open in this case as they come under tension, i.e.,

$$\varphi_2 = \frac{2M_2 l}{Ebt^3(1-\alpha)^3} \tag{30}$$

The rotation of the members AB, BC and BD will be same, i.e., $\varphi_1 = \varphi_2 = \varphi$. This leads us to the relation between M_1 and M_2.

$$M_1(1-\alpha)^3 = M_2 \tag{31}$$

The sum of moments acting on AB and BC will be equal to that acting on BD, i.e., $M_1 + M_2 = M$, which gives the relation between M_1, M_2 and M.

$$M_1 = \frac{M}{1+(1-\alpha)^3} \quad \text{and} \quad M_2 = \frac{M(1-\alpha)^3}{1+(1-\alpha)^3} \tag{32}$$

Using Eq. (25), the rotation of member BD about B, is then given by

$$\varphi = \frac{2Ml}{Ebt^3\left(1+(1-\alpha)^3\right)} = \frac{Flh}{Ebt^3\left(1+(1-\alpha)^3\right)} \tag{33}$$

Under the far-field shear stress τ, along direction-1, the shear deformation due to bending can be given as

$$\begin{aligned}\delta_{1_B} &= 2\left(\varphi\frac{h}{2}+\eta_D\right)\\ &= \frac{Fh^2}{Ebt^3}\left(\frac{l}{1+(1-\alpha)^3}+\frac{h}{(1-\alpha)^3}\right)\end{aligned} \tag{34}$$

The total shear strain is given by

$$\begin{aligned}\gamma &= \frac{\delta_{1_B}}{h+l\sin\theta}\\ &= \frac{Fh^2}{Eb\,(h+l\sin\theta)\,t^3}\left(\frac{l}{1+(1-\alpha)^3}+\frac{h}{(1-\alpha)^3}\right)\\ &= \frac{2\tau h^2\cos\theta}{E\left(\frac{h}{l}+\sin\theta\right)t^3}\left(\frac{l}{1+(1-\alpha)^3}+\frac{h}{(1-\alpha)^3}\right)\end{aligned} \tag{35}$$

The shear modulus is, thus, expressed as

$$\begin{aligned}G_{12}^{-} &= \frac{\tau}{\gamma}\\ &= \left(\frac{t}{l}\right)^3\frac{E\left(\frac{h}{l}+\sin\theta\right)}{2\cos\theta\left(\frac{h}{l}\right)^2\left(\frac{1}{1+(1-\alpha)^3}+\frac{h}{l\,(1-\alpha)^3}\right)}\end{aligned} \tag{36}$$

The direction of shear stress is considered anti-clockwise in the above derivation (refer Fig. 4(B)) and thus we denote the Shear modulus with a negative superscript.

Now, consider the case when the direction of the shear stress reverses (refer Fig. 4(C)). The derivation of shear modulus, G_{12}^{+} (considering clockwise far-field shear stress (refer Fig. 4(C))), where the cuts in the vertical member BD as well as the inclined member BC close while those in the slant member AB open (refer Fig. 4(F–G)). Thus the shear modulus is expressed as

$$G_{12}^{+} = \left(\frac{t}{l}\right)^3\frac{E\left(\frac{h}{l}+\sin\theta\right)}{2\cos\theta\left(\frac{h}{l}\right)^2\left(\frac{1}{1+(1-\alpha)^3}+\frac{h}{l}\right)} \tag{37}$$

It is interesting to observe that when the direction of shear stress is reversed, the shear modulus remains a function of the α, while when the normal stresses are reversed, the Young's Modulus in longitudinal and transverse direction become either independent of it or get dependent on it, depending on the direction of stress applied. Subsequently, the degree of non-invariance for shear modulus can be defined as

$$\frac{G_{12}^{+}}{G_{12}^{-}} = \frac{\left(\frac{1}{1+(1-\alpha)^3}+\frac{h}{l\,(1-\alpha)^3}\right)}{\left(\frac{1}{1+(1-\alpha)^3}+\frac{h}{l}\right)} \tag{38}$$

This above equation shows that the degree of non-invariance for shear moduli under clockwise and anti-clockwise far-field shear stresses depends on α.

2.1.2. *In-plane elastic moduli considering beam-level bending, axial and shear deformations*

In this section, we derive the closed-form expressions of the five in-plane elastic moduli, namely, E_1, ν_{12}, E_2, ν_{21}, and G_{12} including the axial and shear deformation of the cell walls along with the effect of bending deformation that is considered in the preceding section. This is a further generalization of Section 2.1.1, the outcomes of which would show the importance of a more accurate analysis.

2.1.2.1. Longitudinal Young's modulus E_1. From Eq. (2), we have the bending deflection, for unit cell under a far-field compressive stress along direction-1,

$$\delta = \left(\frac{l}{t}\right)^3\frac{P\sin\theta}{bE\,(1-\alpha)^3} \tag{39}$$

The deflection of the member considering the shear effect (Dawe, 1984; Petyt, 1990; Adhikari et al., 2021) is given by

$$\delta_s = \left(\frac{l}{t}\right)^3\frac{P\sin\theta\Phi}{bE\,(1-\alpha)^3} \tag{40}$$

where Φ, which represents the shear effect, is given for full beam thickness t as

$$\Phi = \frac{2\,(1+\nu)}{k}\left(\frac{t}{l}\right)^2 \tag{41}$$

In the present case, since the cuts open, the effective thickness of beam is $t\,(1-\alpha)$. Thus, here $\Phi = \frac{2\,(1+\nu)}{k}\left(\frac{t\,(1-\alpha)}{l}\right)^2$. where k is the shear area coefficient. For solid rectangular sections $k = 5/6$. Thus δ_s for far-field compressive stress in direction 1 is given by

$$\delta_s = \left(\frac{l}{t}\right)\frac{2P\sin\theta\,(1+\nu)}{kbE\,(1-\alpha)} \tag{42}$$

The load P has a component $P\cos\theta$ along the local longitudinal axis of the slant members, which results in axial deformation of the member. The axial deflection is given by

$$\delta_a = \left(\frac{l}{t}\right)\frac{P\cos\theta}{Eb(1-\alpha)} \tag{43}$$

Now, the total deflection along the direction of σ_1 is the sum of deflection due to bending, shear and axial effects, i.e.,

$$\begin{aligned}\delta_1 &= \delta\sin\theta + \delta_s\sin\theta + \delta_a\cos\theta \\ &= \left(\frac{l}{t}\right)\frac{P\sin^2\theta}{Eb(1-\alpha)}\left(\left(\frac{l}{t(1-\alpha)}\right)^2 + \frac{2(1+\nu)}{k} + \cot^2\theta\right)\end{aligned} \tag{44}$$

Then the total strain along direction-1 is given by

$$\begin{aligned}\varepsilon_1 &= \frac{\delta_1}{l\cos\theta} \\ &= \frac{\sigma_1(h + l\sin\theta)\sin^2\theta}{Et(1-\alpha)\cos\theta}\left(\left(\frac{l}{t(1-\alpha)}\right)^2 + \frac{2(1+\nu)}{k} + \cot^2\theta\right)\end{aligned} \tag{45}$$

Thus the Young's modulus for the application of compressive stress σ_1 is given by

$$\begin{aligned}E_1^C &= \frac{\sigma_1}{\varepsilon_1} \\ &= \left(\frac{t}{l}\right)\frac{E(1-\alpha)\cos\theta}{\left(\frac{h}{l} + \sin\theta\right)\sin^2\theta\left(\left(\frac{l}{t(1-\alpha)}\right)^2 + \frac{2(1+\nu)}{k} + \cot^2\theta\right)}\end{aligned} \tag{46}$$

By a similar approach, the Young's modulus under the application of a far-field tensile stress which causes the cuts to close is obtained by putting $\alpha = 0$ in the above equation, i.e.,

$$\begin{aligned}E_1^T &= \frac{\sigma_1}{\varepsilon_1} \\ &= \left(\frac{t}{l}\right)\frac{E\cos\theta}{\left(\frac{h}{l} + \sin\theta\right)\sin^2\theta\left(\left(\frac{l}{t}\right)^2 + \frac{2(1+\nu)}{k} + \cot^2\theta\right)}\end{aligned} \tag{47}$$

The ratio of longitudinal Young's modulus under application of tensile stress to that under application of compressive stress, considering bending, axial and shear deformation, is obtained by using the expressions (47) and (46)

$$\frac{E_1^T}{E_1^C} = \frac{\left(\frac{l}{t(1-\alpha)}\right)^2 + \frac{2(1+\nu)}{k} + \cot^2\theta}{(1-\alpha)\left(\left(\frac{l}{t}\right)^2 + \frac{2(1+\nu)}{k} + \cot^2\theta\right)} \tag{48}$$

This ratio defines the degree of non-invariance for longitudinal Young's moduli under tension and compression, that depends on α.

2.1.2.2. Poisson's ratio ν_{12}. Using the Eq. (39), (42), and (43) for the expressions of the deformation, the total deflection in direction-2, due to the far-field compressive stress applied in the direction-1, is obtained as

$$\begin{aligned}-\delta_2 &= \delta\cos\theta + \delta_s\cos\theta - \delta_a\sin\theta \\ &= \left(\frac{l}{t}\right)\frac{P\sin\theta\cos\theta}{Eb(1-\alpha)}\left(\left(\frac{l}{t(1-\alpha)}\right)^2 + \frac{2(1+\nu)}{k} - 1\right)\end{aligned} \tag{49}$$

Total strain along direction-2 is given as

$$\begin{aligned}-\varepsilon_2 &= \frac{\delta_2}{h + l\sin\theta} \\ &= \frac{P\sin\theta\cos\theta}{Ebt(1-\alpha)\left(\frac{h}{l} + \sin\theta\right)}\left(\left(\frac{l}{t(1-\alpha)}\right)^2 + \frac{2(1+\nu)}{k} - 1\right)\end{aligned} \tag{50}$$

From the Eqs. (45) and (50), the Poisson's ratio ν_{12} for compressive far-field stress can be obtained as

$$\begin{aligned}\nu_{12}^C &= -\frac{\varepsilon_2}{\varepsilon_1} \\ &= \frac{\cos^2\theta\left(\left(\frac{l}{t(1-\alpha)}\right)^2 + \frac{2(1+\nu)}{k} - 1\right)}{\left(\frac{h}{l} + \sin\theta\right)\sin\theta\left(\left(\frac{l}{t(1-\alpha)}\right)^2 + \frac{2(1+\nu)}{k} + \cot^2\theta\right)}\end{aligned} \tag{51}$$

When tensile far-field stress is applied along direction-1, the cuts close and the Poisson's ratio ν_{12} is given by

$$\nu_{12}^T = \frac{\cos^2\theta\left(\left(\frac{l}{t}\right)^2 + \frac{2(1+\nu)}{k} - 1\right)}{\left(\frac{h}{l} + \sin\theta\right)\sin\theta\left(\left(\frac{l}{t}\right)^2 + \frac{2(1+\nu)}{k} + \cot^2\theta\right)} \tag{52}$$

Thus we see that under the effect of compressive stress, the Poisson's ratio ν_{12} is a function of α while under tensile stress, it is independent of α.

The ratio of longitudinal Poisson's ratio under application of tensile stress to that under application of compressive stress, considering bending, axial and shear deformation, is obtained by using the expressions (52) and (51)

$$\frac{\nu_{12}^T}{\nu_{12}^C} = \frac{\left(\left(\frac{l}{t}\right)^2 + \frac{2(1+\nu)}{k} - 1\right)\left(\left(\frac{l}{t(1-\alpha)}\right)^2 + \frac{2(1+\nu)}{k} + \cot^2\theta\right)}{\left(\left(\frac{l}{t(1-\alpha)}\right)^2 + \frac{2(1+\nu)}{k} - 1\right)\left(\left(\frac{l}{t}\right)^2 + \frac{2(1+\nu)}{k} + \cot^2\theta\right)} \tag{53}$$

This ratio defines the degree of non-invariance of longitudinal Poisson's ratio under tension and compression, which depends on α.

2.1.2.3. Transverse Young's modulus E_2. The deflection due to bending under the application of compressive far-field stress σ_2 in direction-2 is given as (refer to Eq. (12))

$$\delta = \left(\frac{l}{t}\right)^3 \frac{W\cos\theta}{bE} \tag{54}$$

The defelection of the member considering the shear effect is given by

$$\delta_s = \left(\frac{l}{t}\right)^3 \frac{W\cos\theta\Phi}{bE} = \left(\frac{l}{t}\right)\frac{2W\cos\theta(1+\nu)}{kbE} \tag{55}$$

The load W has a component $W\sin\theta$ along the longitudinal axis of the slant member, which results in axial deformation of the member. The axial deflection is given by

$$\delta_a = \left(\frac{l}{t}\right)\frac{W\sin\theta}{Eb} \tag{56}$$

Along direction-2, total force on the vertical member is $2W$. Therefore, the axial displacement of the vertical member of length h is

$$\delta_{a_v} = \left(\frac{h}{t}\right)\frac{2W}{Eb} \tag{57}$$

Now, the total defelection along the direction of σ_2 is the sum of deflection due to bending, shear and axial effects, i.e.,

$$\begin{aligned}\delta_2 &= \delta\cos\theta + \delta_s\cos\theta + \delta_a\sin\theta + \delta_{a_v}\\ &= \left(\frac{l}{t}\right)\frac{W\cos^2\theta}{Eb}\left(\left(\frac{l}{t}\right)^2 + \frac{2(1+\nu)}{k} + \tan^2\theta + \frac{2}{\cos^2\theta}\left(\frac{h}{l}\right)\right)\end{aligned} \tag{58}$$

Then the total strain along direction-2 is given by

$$\begin{aligned}\varepsilon_2 &= \frac{\delta_2}{h + l\sin\theta}\\ &= \left(\frac{l}{t}\right)\frac{\sigma_2\cos^3\theta}{E\left(\frac{h}{l} + \sin\theta\right)}\left(\left(\frac{l}{t}\right)^2 + \frac{2(1+\nu)}{k} + \tan^2\theta + \frac{2}{\cos^2\theta}\left(\frac{h}{l}\right)\right)\end{aligned} \tag{59}$$

Thus the Young's modulus along the application of compressive stress σ_2 is given by

$$\begin{aligned}E_2^C &= \frac{\sigma_2}{\varepsilon_2}\\ &= \left(\frac{t}{l}\right)\frac{E\left(\frac{h}{l} + \sin\theta\right)}{\cos^3\theta\left(\left(\frac{l}{t}\right)^2 + \frac{2(1+\nu)}{k} + \tan^2\theta + \frac{2}{\cos^2\theta}\left(\frac{h}{l}\right)\right)}\end{aligned} \tag{60}$$

Similarly, if a uniform tensile far-field stress σ_2 is applied along direction-2 for calculation of transverse Young's Modulus, the cuts in the unit cell open up as they now come under tension. The deflection due to bending is given by (refer to Eq. (16))

$$\delta = \left(\frac{l}{t}\right)^3 \frac{W\cos\theta}{bE(1-\alpha)^3} \tag{61}$$

The defelection of the member considering the shear effect is given by

$$\delta_s = \left(\frac{l}{t}\right)\frac{2W\cos\theta}{kbE(1-\alpha)(1+\nu)} \tag{62}$$

The load W has a component $W\sin\theta$ along the longitudinal axis of the slant member, which results in axial deformation of the slant member. The axial deflection is given by

$$\delta_a = \left(\frac{l}{t}\right)\frac{W\sin\theta}{Eb(1-\alpha)} \tag{63}$$

The total force acting in the direction-2 on the vertical member is $2W$. Under tensile stress, the cuts open; therefore, the axial displacement of the vertical member of length h is

$$\delta_{a_v} = \left(\frac{h}{t(1-\alpha)}\right)\frac{2W}{Eb} \tag{64}$$

Now, the total defelection along the direction of σ_2 is the sum of deflection due to bending, shear and axial effects, i.e.,

$$\begin{aligned}\delta_2 &= \delta\cos\theta + \delta_s\cos\theta + \delta_a\sin\theta + \delta_{a_v}\\ &= \left(\frac{l}{t}\right)\frac{W\cos^2\theta}{Eb(1-\alpha)}\left(\left(\frac{l}{t(1-\alpha)}\right)^2 + \frac{2(1+\nu)}{k} + \tan^2\theta + \frac{2}{\cos^2\theta}\left(\frac{h}{l}\right)\right)\end{aligned} \tag{65}$$

Strain along direction of σ_2 is, therefore, given as

$$\begin{aligned}\varepsilon_2 &= \frac{\delta_2}{h + l\sin\theta} \\ &= \frac{W\cos^2\theta}{Eb\left(\frac{h}{l}+\sin\theta\right)t(1-\alpha)}\left(\left(\frac{l}{t(1-\alpha)}\right)^2 + \frac{2(1+\nu)}{k} + \tan^2\theta + \frac{2}{\cos^2\theta}\left(\frac{h}{l}\right)\right) \\ &= \left(\frac{l}{t}\right)\frac{\sigma_2\cos^3\theta}{E\left(\frac{h}{l}+\sin\theta\right)(1-\alpha)}\left(\left(\frac{l}{t(1-\alpha)}\right)^2 + \frac{2(1+\nu)}{k} + \tan^2\theta + \frac{2}{\cos^2\theta}\left(\frac{h}{l}\right)\right)\end{aligned} \tag{66}$$

Thus, the transverse Young's modulus, under application of tensile far-field stress, can be expressed in closed-form as

$$E_2^T = \left(\frac{t}{l}\right)\frac{E\left(\frac{h}{l}+\sin\theta\right)(1-\alpha)}{\cos^3\theta\left(\left(\frac{l}{t(1-\alpha)}\right)^2 + \frac{2(1+\nu)}{k} + \tan^2\theta + \frac{2}{\cos^2\theta}\left(\frac{h}{l}\right)\right)} \tag{67}$$

The ratio of transverse Young's modulus under application of tensile stress to that under application of compressive stress, considering bending, axial and shear deformation, is obtained by using the expressions (67) and (60)

$$\frac{E_2^T}{E_2^C} = \frac{(1-\alpha)\left(\left(\frac{l}{t}\right)^2 + \frac{2(1+\nu)}{k} + \tan^2\theta + \frac{2}{\cos^2\theta}\left(\frac{h}{l}\right)\right)}{\left(\frac{l}{t(1-\alpha)}\right)^2 + \frac{2(1+\nu)}{k} + \tan^2\theta + \frac{2}{\cos^2\theta}\left(\frac{h}{l}\right)} \tag{68}$$

This ratio defines the degree of non-invariance of transverse Young's moduli under tension and compression, which depends on α.

2.1.2.4. Poisson's ratio ν_{21}. Using Eq. (54), (55), and (56) for the formulations of the deformation, the total deflection in longitudinal direction, under the compressive far-field stress acting along direction-2, is obtained as

$$\begin{aligned}-\delta_1 &= \delta\sin\theta + \delta_s\sin\theta - \delta_a\cos\theta \\ &= \left(\frac{l}{t}\right)\frac{W\sin\theta\cos\theta}{Eb}\left(\left(\frac{l}{t}\right)^2 + \frac{2(1+\nu)}{k} - 1\right)\end{aligned} \tag{69}$$

In the transverse direction, the total strain is expressed as

$$\begin{aligned}-\varepsilon_1 &= \frac{\delta_1}{l\cos\theta} \\ &= \frac{W\sin\theta}{Ebt}\left(\left(\frac{l}{t}\right)^2 + \frac{2(1+\nu)}{k} - 1\right)\end{aligned} \tag{70}$$

From Eq. (59) and Eq. (70), the Poisson's ratio ν_{12} can be expressed as

$$\begin{aligned}\nu_{21}^C &= -\frac{\varepsilon_1}{\varepsilon_2} \\ &= \frac{\sin\theta\left(\frac{h}{l}+\sin\theta\right)\left(\left(\frac{l}{t}\right)^2 + \frac{2(1+\nu)}{k} - 1\right)}{\cos^2\theta\left(\left(\frac{l}{t}\right)^2 + \frac{2(1+\nu)}{k} + \tan^2\theta + \frac{2}{\cos^2\theta}\left(\frac{h}{l}\right)\right)}\end{aligned} \tag{71}$$

Following a similar approach as above, when far-field tensile stress is applied along direction-2, the cuts open and the Poisson's ratio ν_{21} is given by

$$\nu_{21}^T = \frac{\sin\theta\left(\frac{h}{l}+\sin\theta\right)\left(\left(\frac{l}{t(1-\alpha)}\right)^2 + \frac{2(1+\nu)}{k} - 1\right)}{\cos^2\theta\left(\left(\frac{l}{t(1-\alpha)}\right)^2 + \frac{2(1+\nu)}{k} + \tan^2\theta + \frac{2}{\cos^2\theta}\left(\frac{h}{l}\right)\right)} \tag{72}$$

Thus we see that under the effect of compressive stress, the Poisson's ratio ν_{21} is independent of α while under tensile stress, it is a function of α.

The ratio of transverse Poisson's ratio under application of tensile stress to that under application of compressive stress, considering bending, axial and shear deformation, is obtained by using the expressions (72) and (71)

$$\frac{\nu_{21}^T}{\nu_{21}^C} = \frac{\left(\left(\frac{l}{t(1-\alpha)}\right)^2 + \frac{2(1+\nu)}{k} - 1\right)\left(\left(\frac{l}{t}\right)^2 + \frac{2(1+\nu)}{k} + \tan^2\theta + \frac{2}{\cos^2\theta}\left(\frac{h}{l}\right)\right)}{\left(\left(\frac{l}{t}\right)^2 + \frac{2(1+\nu)}{k} - 1\right)\left(\left(\frac{l}{t(1-\alpha)}\right)^2 + \frac{2(1+\nu)}{k} + \tan^2\theta + \frac{2}{\cos^2\theta}\left(\frac{h}{l}\right)\right)} \tag{73}$$

This ratio defines the degree of non-invariance of transverse Poisson's ratio under tension and compression, which depends on α.

2.1.2.5. Shear modulus G_{12}. First we consider the case when far-field shear stress is applied in the anti-clockwise direction. To derive of the shear modulus G_{12}, we consider the shear strain arising from the bending deformations as well as that due to axial and shear deformations. The vertical cell wall is considered to have length $h/2$ (noting that the bending moment at the mid-point is zero), while the slant cell walls have length l and

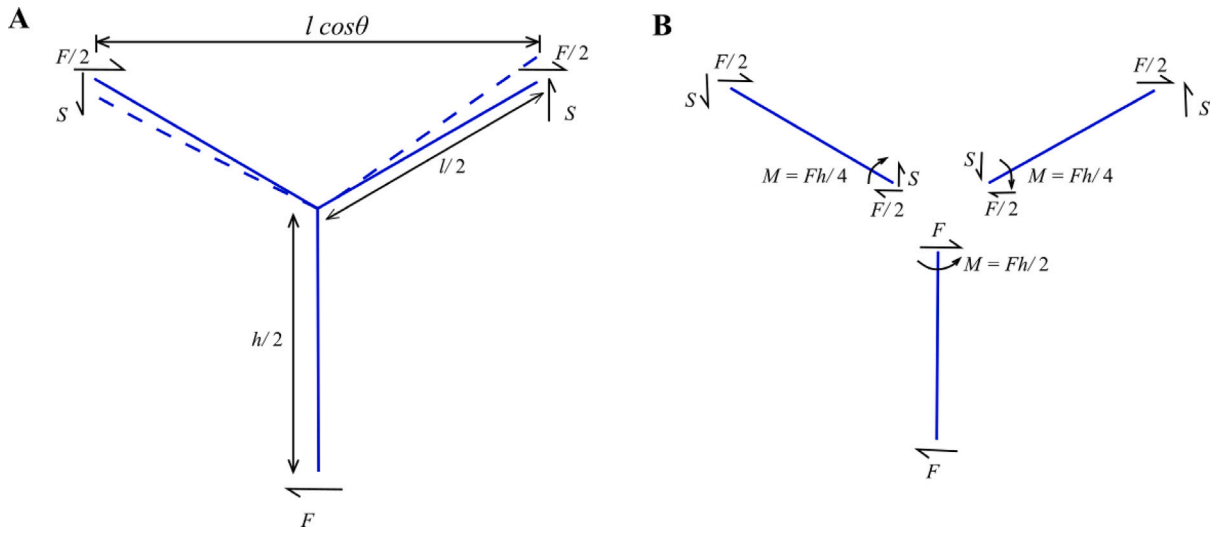

Fig. 5. Strain calculation of the shear modulus considering axial and shear deformation. (A) Forces acting on unit cell in shear. The deformation in the oblique members is shown using dashed lines. **(B)** Equilibrium of unit cell in shear.

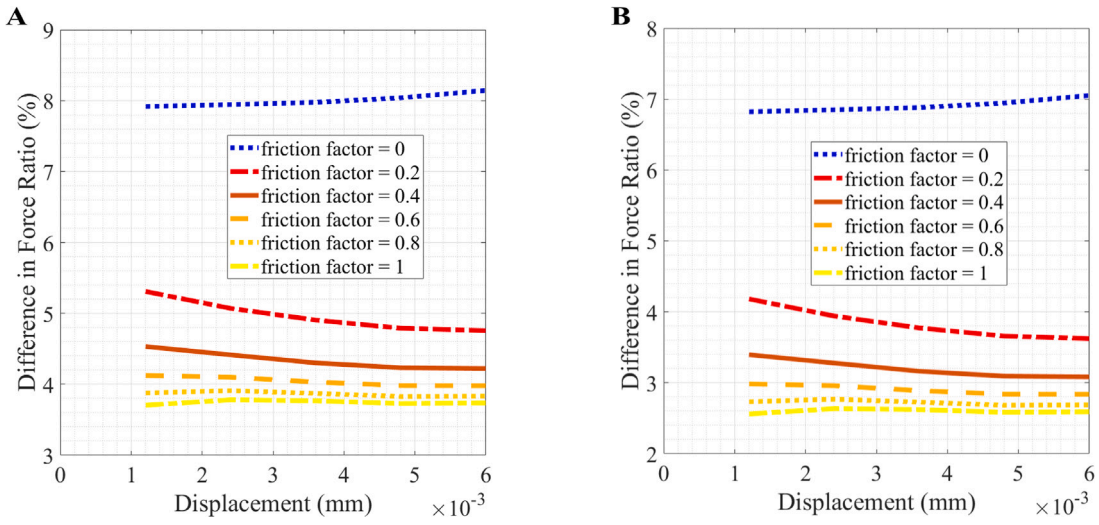

Fig. 6. Numerical Validation for a beam element with domain discontinuity. (A) Validation of the beam element by analyzing the percentage error between theoretical results and finite element results considering bending deformation for different values of deflection. **(B)** Validation of the beam element by analyzing the percentage error between theoretical results and finite element results considering both bending and shear deformations for different values of deflection. The dimensions of the beam used are, length 70 mm, width 5 mm and height 5 mm. The intrinsic material properties are taken as $E = 2 \times 10^{11}$ and Poisson's ratio $\nu = 0.3$. Finite element analysis is carried out considering different friction factors and load values.

inclination angle is θ. Under anti-clockwise shear stress field, the cuts of the vertical member BD and the slant member BC open while that of AB close. The force due to shear stress is F along direction-1 and S along direction-2 (refer to Fig. 5). The shear stress field produces forces F_1 and F_2 in the slant members. The forces F and S are given as

$$F = 2\tau bl\cos\theta \tag{74a}$$

$$S = \tau b\,(h + l\sin\theta) \tag{74b}$$

The force produced in the vertical cell member is given as

$$F_v = F = 2\tau bl\cos\theta \tag{75}$$

The moment M generated in the vertical member is given as

$$M = \frac{Fh}{2} \tag{76}$$

No axial force is produced in the vertical cell wall under the applied shear stress. This moment M gets distributed in the two slant members. Note that the moment M does not get distributed equally on the two slant cell walls since the cuts in member AB close while that in member BC open. The moment generated on slant member AB is denoted by M_1 while that on the slant member BC is M_2. The sum of the two moments is equal to M, i.e., $M = M_1 + M_2$. The different moments in the two slant members due to closing and opening of cuts makes it an asymmetric problem. The force F gets distributed on both the slant members as F_1 and F_2 such that $F = F_1 + F_2$. We use the compatibility condition that the joint rotation of the vertical cell wall and that of the slant members will be equal, i.e., $\phi = \phi_1 = \phi_2$. Here ϕ_1 and ϕ_2 are the rotations of the slant members,

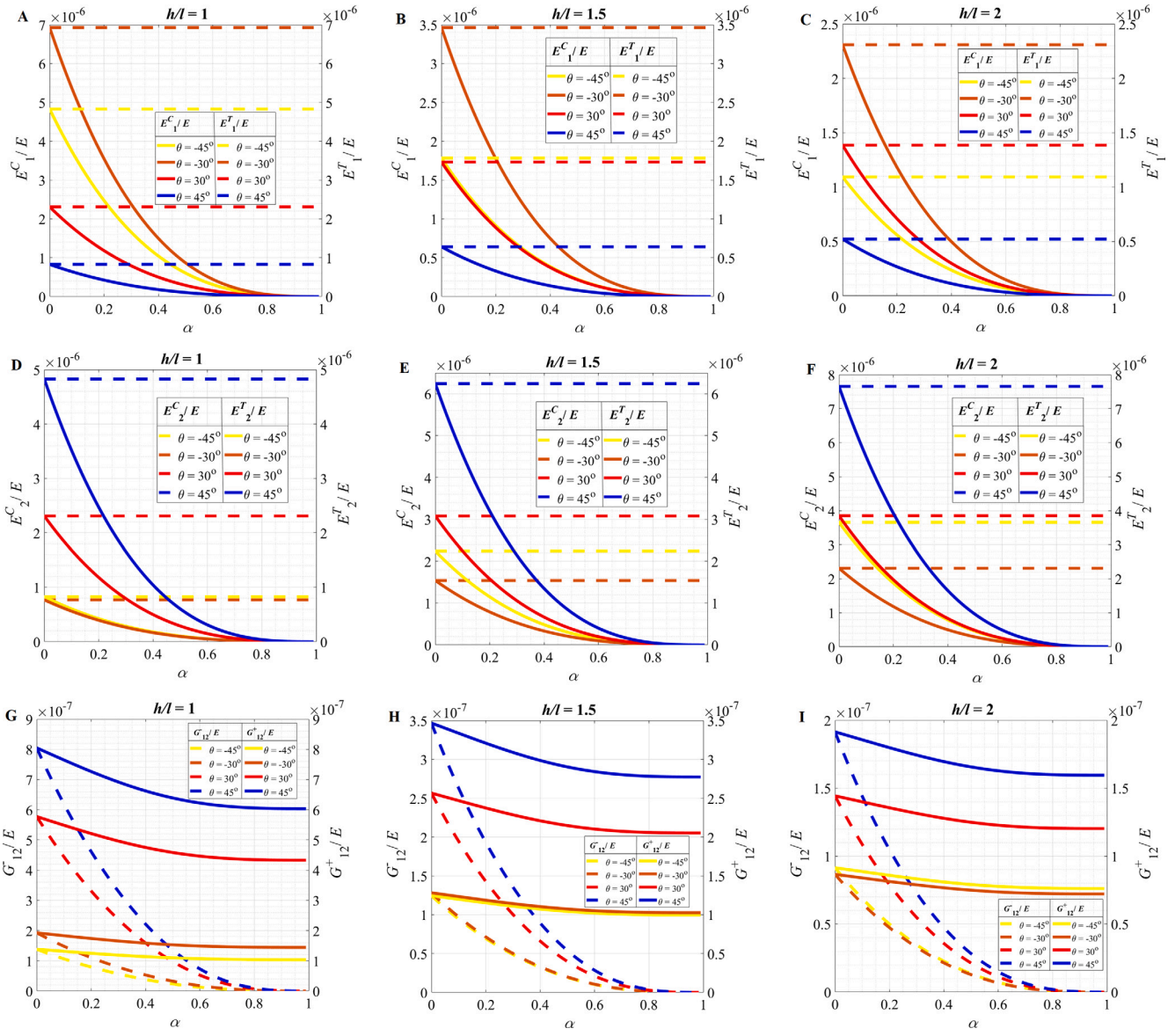

Fig. 7. Non-invariant elastic moduli for hexagonal lattices considering only beam-level bending deformation. (A–C) Variation of non-dimensionalized Young's modulus in longitudinal direction, i.e., E_1/E, with the ratio of depth of cut to total thickness of cell wall, α, for different values of θ and h/l. **(D–F)** Variation of non-dimensionalized Young's modulus in transverse direction, i.e., E_2/E, with the ratio of depth of cut to total thickness of cell wall, α, for different values of θ and h/l. **(G–I)** Variation of non-dimensionalized shear modulus, i.e., G_{12}/E, with the ratio of depth of cut to total thickness of cell wall, α, for different values of θ and h/l. Note that these elastic moduli are calculated considering Configuration 1 of domain discontinuity.

which are given as

$$\phi_1 = \tan^{-1}\left(\delta_{y_1}/l\right) \approx \left(\delta_{y_1}/l\right) \text{ and } \phi_2 = \tan^{-1}\left(\delta_{y_2}/l\right) \approx \left(\delta_{y_2}/l\right) \tag{77}$$

where δ_{y_1} and δ_{y_2} contains the bending and shear deformations of the slant members AB and BC, respectively, which are given as

$$\delta_{y_1} = \frac{2M_1\left(1 + \frac{2(1+\nu)}{k}\left(\frac{t}{l}\right)^2\right)l^2}{Ebt^3} \tag{78a}$$

$$\delta_{y_2} = \frac{2M_2\left(1 + \frac{2(1+\nu)}{k}\left(\frac{t(1-\alpha)}{l}\right)^2\right)l^2}{Ebt^3(1-\alpha)^3} \tag{78b}$$

Note that the two slant beams are fixed at one end while the other is rotationally restrained. This boundary condition gives us the deformations of AB and BC based on lattice-level deformation behavior. Using $\phi_1 = \phi_2$, we get the relation between M_1 and M_2 as

$$M_1\left(1 + \frac{2(1+\nu)}{k}\left(\frac{t}{l}\right)^2\right)(1-\alpha)^3 = M_2\left(1 + \frac{2(1+\nu)}{k}\left(\frac{t(1-\alpha)}{l}\right)^2\right) \tag{79}$$

Now, using $M = M_1 + M_2$, we obtain M_1 and M_2 in terms of M.

$$M = M_1\left(1+\frac{\left(1+\frac{2(1+\nu)}{k}\left(\frac{t}{l}\right)^2\right)(1-\alpha)^3}{\left(1+\frac{2(1+\nu)}{k}\left(\frac{t(1-\alpha)}{l}\right)^2\right)}\right) = M_2\left(1+\frac{\left(1+\frac{2(1+\nu)}{k}\left(\frac{t(1-\alpha)}{l}\right)^2\right)}{\left(1+\frac{2(1+\nu)}{k}\left(\frac{t}{l}\right)^2\right)(1-\alpha)^3}\right) \tag{80}$$

Since $\phi = \phi_1 = \phi_2$, we have

$$\begin{aligned}\phi = \phi_1 = \left(\delta_{y_1}/l\right) &= \frac{2M_1\left(1+\frac{2(1+\nu)}{k}\left(\frac{t}{l}\right)^2\right)l}{Ebt^3}\\ &= \frac{2Ml\left(1+\frac{2(1+\nu)}{k}\left(\frac{t}{l}\right)^2\right)}{Ebt^3\left(1+\frac{\left(1+\frac{2(1+\nu)}{k}\left(\frac{t}{l}\right)^2\right)(1-\alpha)^3}{\left(1+\frac{2(1+\nu)}{k}\left(\frac{t(1-\alpha)}{l}\right)^2\right)}\right)}\\ &= \frac{Fhl\left(1+\frac{2(1+\nu)}{k}\left(\frac{t}{l}\right)^2\right)}{Ebt^3\left(1+\frac{\left(1+\frac{2(1+\nu)}{k}\left(\frac{t}{l}\right)^2\right)(1-\alpha)^3}{\left(1+\frac{2(1+\nu)}{k}\left(\frac{t(1-\alpha)}{l}\right)^2\right)}\right)}\end{aligned} \tag{81}$$

Along direction-1, the deformation of point D due to bending and shear effects with respect to point B, considering a member of $h/2$ length, is expressed as (considering the boundary conditions for a cantilever beam of length $h/2$ acted upon by a force F at free end)

$$\eta_D = \frac{12F\left(\frac{h}{2}\right)^3}{Ebt^3(1-\alpha)^3}\left(\frac{1+\frac{2(1+\nu)}{k}\left(\frac{2t(1-\alpha)}{h}\right)^2}{12-\frac{36}{4+\frac{2(1+\nu)}{k}\left(\frac{2t(1-\alpha)}{h}\right)^2}}\right) \tag{82}$$

Thus the shear strain γ_v due to beam-level bending and shear deformations is given as

$$\gamma_v = \frac{2\left(\phi\frac{h}{2}+\eta_D\right)}{h+l\sin\theta} \tag{83}$$

We have F_1 and F_2 acting on the two slant slant members AB and BC, respectively. These forces are related to the moments M_1 and M_2, which is given as

$$M_1 = \frac{\left(S\cos\theta - F_1\sin\theta\right)l}{2} \text{ and } M_2 = \frac{\left(S\cos\theta - F_2\sin\theta\right)l}{2} \tag{84}$$

The above equation when solved in conjunction with the condition that $F = F_1 + F_2$, we obtain

$$F_1 = \frac{F}{2} - \frac{\left(M_1 - M_2\right)}{l\sin\theta} \text{ and } F_2 = \frac{F}{2} + \frac{\left(M_1 - M_2\right)}{l\sin\theta} \tag{85}$$

The axial deformation of the slant member AB is given as

$$\begin{aligned}\delta_{x_1} &= \frac{\left(F_1\cos\theta + S\sin\theta\right)l}{Ebt}\\ &= \frac{\left(\frac{Fl}{2} - \frac{\left(M_1 - M_2\right)}{\sin\theta}\right)\cos\theta + Sl\sin\theta}{Ebt}\\ &= \frac{F\cot\theta}{2Ebt}\left(h + l\sin\theta - 2h\left(1+\frac{\left(1+\frac{2(1+\nu)}{k}\left(\frac{t}{l}\right)^2\right)(1-\alpha)^3}{\left(1+\frac{2(1+\nu)}{k}\left(\frac{t(1-\alpha)}{l}\right)^2\right)}\right)^{-1}\right) + \frac{Sl\sin\theta}{Ebt}\end{aligned} \tag{86}$$

Similarly, the axial deformation of the slant member BC is given as

$$\begin{aligned}\delta_{x_2} &= \frac{\left(F_2\cos\theta + S\sin\theta\right)l}{Ebt\left(1-\alpha\right)}\\ &= \frac{\left(\frac{Fl}{2}+\frac{\left(M_1-M_2\right)}{\sin\theta}\right)\cos\theta + Sl\sin\theta}{Ebt\left(1-\alpha\right)}\\ &= \frac{F\cot\theta}{2Ebt\left(1-\alpha\right)}\left(l\sin\theta - h + 2h\left(1+\frac{\left(1+\frac{2\left(1+\nu\right)}{k}\left(\frac{t}{l}\right)^2\right)\left(1-\alpha\right)^3}{\left(1+\frac{2\left(1+\nu\right)}{k}\left(\frac{t\left(1-\alpha\right)}{l}\right)^2\right)}\right)^{-1}\right) + \frac{Sl\sin\theta}{Ebt\left(1-\alpha\right)}\end{aligned} \tag{87}$$

The shear strain γ_s due to beam-level axial deformation is given as

$$\gamma_s = \frac{\delta_{x_1}\sin\theta + \delta_{x_2}\sin\theta}{l\cos\theta} + \frac{\delta_{x_1}\cos\theta + \delta_{x_2}\cos\theta}{h + l\sin\theta} \tag{88}$$

The total shear strain γ_t is therefore given by

$$\begin{aligned}\gamma_t = \gamma_v + \gamma_s &= \frac{2\left(\phi\frac{h}{2}+\eta_D\right)+\delta_{x_1}\cos\theta+\delta_{x_2}\cos\theta}{h+l\sin\theta} + \frac{\delta_{x_1}\sin\theta+\delta_{x_2}\sin\theta}{l\cos\theta}\\ &= \frac{2\tau\left(\frac{h}{l}\right)^2\cos\theta\left(1+\frac{2\left(1+\nu\right)}{k}\left(\frac{t}{l}\right)^2\right)}{E\left(\frac{t}{l}\right)^3\left(\frac{h}{l}+\sin\theta\right)\left(1+\frac{\left(1+\frac{2\left(1+\nu\right)}{k}\left(\frac{t}{l}\right)^2\right)\left(1-\alpha\right)^3}{\left(1+\frac{2\left(1+\nu\right)}{k}\left(\frac{t\left(1-\alpha\right)}{l}\right)^2\right)}\right)}\\ &+ \frac{6\tau\left(\frac{h}{l}\right)^3\cos\theta}{E\left(\frac{t\left(1-\alpha\right)}{l}\right)^3\left(\frac{h}{l}+\sin\theta\right)}\left(\frac{1+\frac{2\left(1+\nu\right)}{k}\left(\frac{2t\left(1-\alpha\right)}{h}\right)^2}{12-\frac{36}{4+\frac{2\left(1+\nu\right)}{k}\left(\frac{2t\left(1-\alpha\right)}{h}\right)^2}}\right)\\ &+ \frac{\tau\cos\theta}{E\left(\frac{t}{l}\right)}\left(1+\frac{\cos\theta\cot\theta}{\left(\frac{h}{l}+\sin\theta\right)}\right)\left(\left(\frac{h}{l}\right)\left(1-\frac{1}{\left(1-\alpha\right)}\right)\right.\\ &+ \sin\theta\left(1+\frac{1}{\left(1-\alpha\right)}\right)+2\left(\frac{h}{l}\right)\left(1+\frac{\left(1+\frac{2\left(1+\nu\right)}{k}\left(\frac{t}{l}\right)^2\right)\left(1-\alpha\right)^3}{\left(1+\frac{2\left(1+\nu\right)}{k}\left(\frac{t\left(1-\alpha\right)}{l}\right)^2\right)}\right)^{-1}\left.\left(\frac{1}{\left(1-\alpha\right)}-1\right)\right)\\ &+ \frac{\tau\sin\theta\cos\theta}{E\left(\frac{t}{l}\right)}\left(1+\frac{1}{\left(1-\alpha\right)}\right)+\frac{2\tau\sin\theta\tan\theta\left(\frac{h}{l}+\sin\theta\right)}{E\left(\frac{t}{l}\right)}\end{aligned} \tag{89}$$

The shear modulus under anti-clockwise shear stress is given by

$$\begin{aligned}G_{12}^{-} &= \frac{\tau}{\gamma_t}\\ &= \frac{Eg_t}{2\cos\theta\left(\begin{array}{c}\left(\frac{g_h^2\left(1+\Phi_l\right)}{g_t^2\left(g_h+\sin\theta\right)}+g_h\left(1+\frac{\cos\theta\cot\theta}{\left(g_h+\sin\theta\right)}\right)\left(\frac{\alpha}{\left(1-\alpha\right)}\right)\right)\frac{1}{\left(1+\frac{\left(1+\Phi_l\right)\left(1-\alpha\right)^3}{1+\Phi_l\left(1-\alpha\right)^2}\right)}\\ +\frac{3g_h^3}{g_t^2\left(1-\alpha\right)^3\left(g_h+\sin\theta\right)}\left(\frac{1+\Phi_h\left(1-\alpha\right)^2}{12-\frac{36}{4+\Phi_h\left(1-\alpha\right)^2}}\right)+\frac{\sin\theta}{2}\left(\frac{2-\alpha}{1-\alpha}\right)+\left(\tan^2\theta\left(g_h+\sin\theta\right)\right)\\ +\frac{1}{2}\left(1+\frac{\cos\theta\cot\theta}{\left(g_h+\sin\theta\right)}\right)\left(g_h\left(\frac{\alpha}{\left(\alpha-1\right)}\right)+\sin\theta\left(\frac{2-\alpha}{1-\alpha}\right)\right)\end{array}\right)}\end{aligned} \tag{90}$$

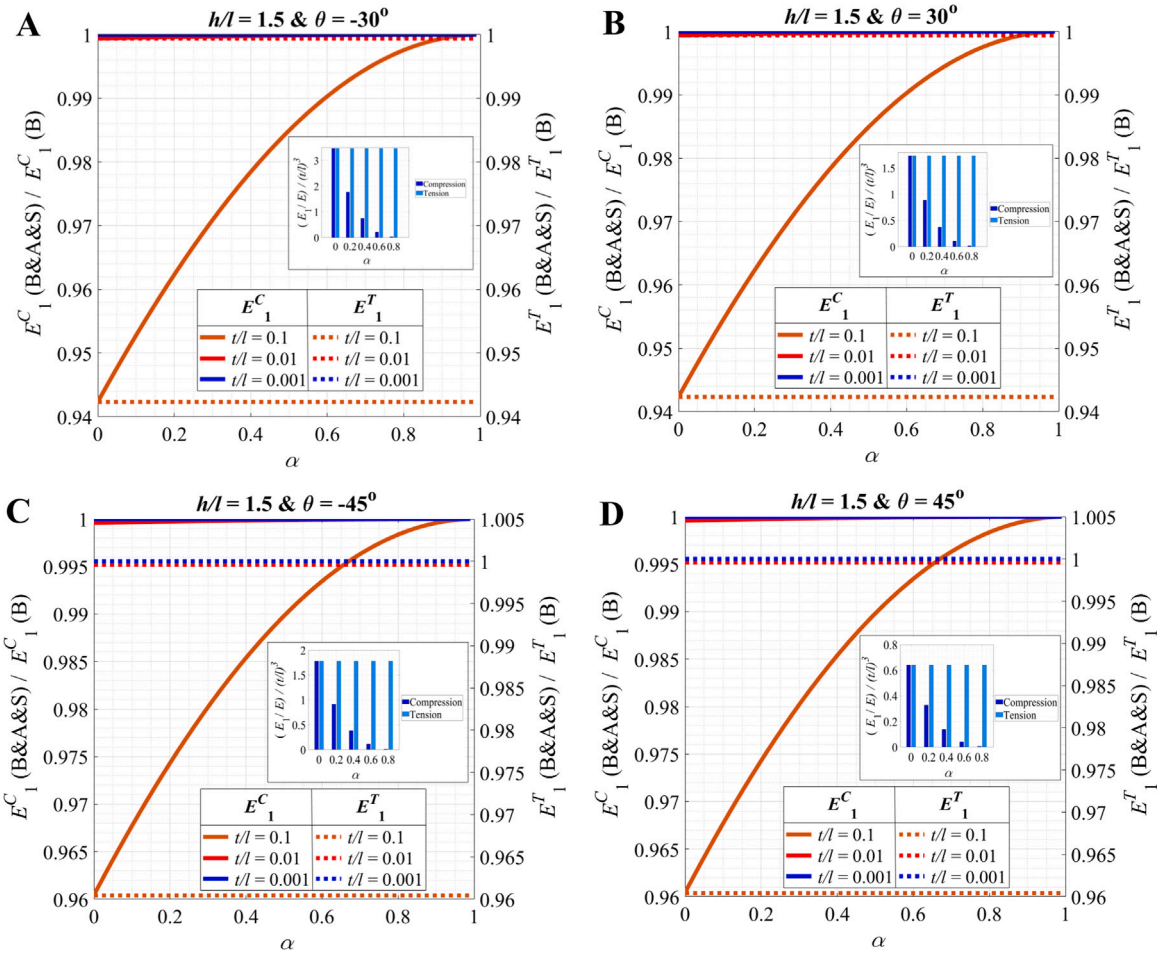

Fig. 8. Effect of beam-level shear and axial deformation on longitudinal Young's modulus. (A–D) Variation of ratio of Young's modulus, considering bending, axial and shear deformations (denoted by B, A and S, respectively, in figure) to the Young's modulus, considering only bending deformation with the ratio of depth of cut to total thickness of cell wall, α, for different auxetic and non-auxetic configurations. The figures in inset show the variation of non-dimensionalized Young's modulus to α, considering only bending deformation, for the unit cell subjected to compressive as well as tensile stresses. Note that the main plot here is intended to show the effect of beam-level axial and shear deformations with respect to only bending deformation. The inset plots give the variation trend of the Young's modulus with α. In each of the subplots, the Young's modulus is presented for compressive and tensile modes of far-field stresses considering the Configuration 1 of domain discontinuity.

where g_t, g_h, ϕ_l and ϕ_h are non-dimensional parameters defined as

$$g_t = \frac{t}{l} \tag{91a}$$

$$g_h = \frac{h}{l} \tag{91b}$$

$$\boldsymbol{\Phi}_l = \frac{2(1+\nu)}{k}\left(\frac{t}{l}\right)^2 \tag{91c}$$

$$\boldsymbol{\Phi}_h = \frac{2(1+\nu)}{k}\left(\frac{2t}{h}\right)^2 \tag{91d}$$

Similarly, when the direction of shear stress is reversed, the cuts of members BC and BD come under compression and thus close, while that of AB open. The shear modulus under clockwise shear stress is then given by

$$G_{12}^{+} = \frac{\tau}{\gamma_t} = \frac{Eg_t}{2\cos\theta\left(\begin{array}{l}\left(\dfrac{g_h^2\left(1+\boldsymbol{\Phi}_l(1-\alpha)^2\right)}{g_t^2(1-\alpha)^3\left(g_h+\sin\theta\right)}+g_h\left(1+\dfrac{\cos\theta\cot\theta}{\left(g_h+\sin\theta\right)}\right)\left(\dfrac{\alpha}{(\alpha-1)}\right)\right)\dfrac{1}{\left(1+\dfrac{1+\boldsymbol{\Phi}_l(1-\alpha)^2}{(1+\boldsymbol{\Phi}_l)(1-\alpha)^3}\right)}\\ +\dfrac{3g_h^3}{g_t^2\left(g_h+\sin\theta\right)}\left(\dfrac{1+\boldsymbol{\Phi}_h}{12-\dfrac{36}{4+\boldsymbol{\Phi}_h}}\right)+\dfrac{\sin\theta}{2}\left(\dfrac{2-\alpha}{1-\alpha}\right)+\left(\dfrac{1}{2}\tan^2\theta\left(g_h+\sin\theta\right)\left(\dfrac{2-\alpha}{1-\alpha}\right)\right)\\ +\dfrac{1}{2}\left(1+\dfrac{\cos\theta\cot\theta}{\left(g_h+\sin\theta\right)}\right)\left(g_h\left(\dfrac{\alpha}{\alpha-1}\right)+\sin\theta\left(\dfrac{2-\alpha}{1-\alpha}\right)\right)\end{array}\right)} \tag{92}$$

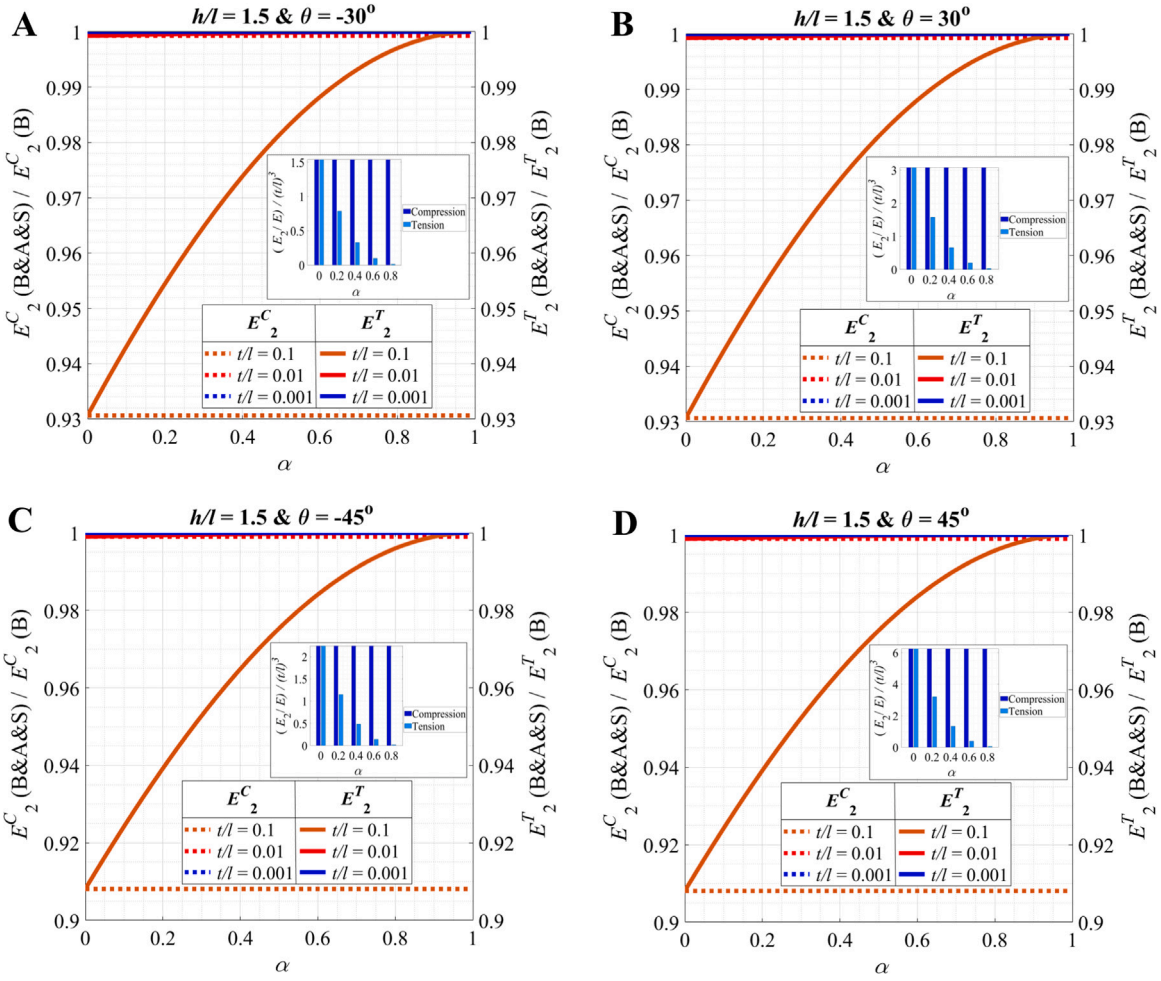

Fig. 9. Effect of beam-level shear and axial deformation on transverse Young's modulus. (A–D) Variation of ratio of Young's modulus, considering bending, axial and shear deformations (denoted by B, A and S, respectively, in figure) to the Young's modulus, considering only bending deformation with the ratio of depth of cut to total thickness of cell wall, α, for different auxetic and non-auxetic configurations. The figures in inset show the variation of non-dimensionalized Young's modulus to α, considering only bending deformation, for the unit cell subjected to compressive as well as tensile stresses. Note that the main plot here is intended to show the effect of beam-level axial and shear deformations with respect to only bending deformation. The inset plots give the variation trend of the Young's modulus with α. In each of the subplots, the Young's modulus is presented for compressive and tensile modes of far-field stresses considering the Configuration 1 of domain discontinuity.

The ratio of shear modulus under application of clockwise shear stress to that under application of anticlockwise shear stress is obtained by using the expressions (90) and (92)

$$\frac{G_{12}^{+}}{G_{12}^{-}}=\frac{\left(\begin{array}{l}\left(\frac{g_h^2\left(1+\Phi_l\right)}{g_t^2\left(g_h+\sin\theta\right)}+g_h\left(1+\frac{\cos\theta\cot\theta}{\left(g_h+\sin\theta\right)}\right)\left(\frac{\alpha}{(1-\alpha)}\right)\right)\frac{1}{\left(1+\frac{\left(1+\Phi_l\right)(1-\alpha)^3}{1+\Phi_l(1-\alpha)^2}\right)}\\+\frac{3g_h^3}{g_t^2(1-\alpha)^3\left(g_h+\sin\theta\right)}\left(\frac{1+\Phi_h(1-\alpha)^2}{12-\frac{36}{4+\Phi_h(1-\alpha)^2}}\right)+\frac{\sin\theta}{2}\left(\frac{2-\alpha}{1-\alpha}\right)+\left(\tan^2\theta\left(g_h+\sin\theta\right)\right)\\+\frac{1}{2}\left(1+\frac{\cos\theta\cot\theta}{\left(g_h+\sin\theta\right)}\right)\left(g_h\left(\frac{\alpha}{(\alpha-1)}\right)+\sin\theta\left(\frac{2-\alpha}{1-\alpha}\right)\right)\end{array}\right)}{\left(\begin{array}{l}\left(\frac{g_h^2\left(1+\Phi_l(1-\alpha)^2\right)}{g_t^2(1-\alpha)^3\left(g_h+\sin\theta\right)}+g_h\left(1+\frac{\cos\theta\cot\theta}{\left(g_h+\sin\theta\right)}\right)\left(\frac{\alpha}{(\alpha-1)}\right)\right)\frac{1}{\left(1+\frac{1+\Phi_l(1-\alpha)^2}{\left(1+\Phi_l\right)(1-\alpha)^3}\right)}\\+\frac{3g_h^3}{g_t^2\left(g_h+\sin\theta\right)}\left(\frac{1+\Phi_h}{12-\frac{36}{4+\Phi_h}}\right)+\frac{\sin\theta}{2}\left(\frac{2-\alpha}{1-\alpha}\right)+\left(\frac{1}{2}\tan^2\theta\left(g_h+\sin\theta\right)\left(\frac{2-\alpha}{1-\alpha}\right)\right)\\+\frac{1}{2}\left(1+\frac{\cos\theta\cot\theta}{\left(g_h+\sin\theta\right)}\right)\left(g_h\left(\frac{\alpha}{\alpha-1}\right)+\sin\theta\left(\frac{2-\alpha}{1-\alpha}\right)\right)\end{array}\right)} \tag{93}$$

This ratio defines the degree of non-invariance of shear moduli under clockwise and anticlockwise shear stress, which depends on α.

2.2. In-plane elastic properties of Configuration 2

Here we will consider the cases when the position of cuts interchange, i.e., those on convex curvature of deformed unit cell member are now considered on the concave side and vice-versa. We first discuss here some of the general trends that become evident from the expressions of elastic moduli presented in this paper. When only beam-level bending deformation is considered, the expressions for all the elastic moduli for Configuration 2 interchange for compressive and tensile stresses or clockwise and anti-clockwise shear stresses with respect to the Configuration 1. However, when beam-level bending axial and shear deformations are considered, such interchange may or may not hold good, depending on the elastic property under consideration.

In this paragraph, we discuss the elastic moduli when combined effect of beam-level bending, axial and shear deformations are considered. It can be observed that in such configuration, the longitudinal Young's modulus E_1 and Poisson's ratio ν_{12} under compression will be same as those under tension in Configuration 1 which are discussed in the following subsections. Similarly these elastic properties (E_1 and ν_{12}) under tension will be same as those under compression in Configuration 1. An interesting point to note here is that it does not go with transverse Young's modulus E_2 and Poisson's ratio ν_{21}. Their expressions under tension and compression will change in different configurations due to the effect of α. This effect is observed in the final expressions of E_2 and ν_{21}, which are different under compression in Configuration 1 and under tension in Configuration 2 and vice-versa. For the case of shear modulus, the expression of anticlockwise shear modulus G_{12}^{-} in Configuration 1 will be similar to the clockwise shear modulus G_{12}^{+} in Configuration 2 and vice-versa. This is because in Configuration 1, the cuts of the vertical member BD and slant member BC open up under anticlockwise shear stress while that of slant member AB close. While in Configuration 2, the similar conditions are observed under clockwise shear stress. Thus we can deduce that the changes in the expressions of the elastic moduli under different configurations are due to the effect of α.

In the following subsections, we have presented the closed-form expressions of the five elastic moduli under tensile and compressive far-field stresses considering the Configuration 2. For each case, we have shown the expressions considering only beam-level bending deformation and compound effects of bending, axial and shear deformations, separately.

2.2.1. Longitudinal Young's modulus E_1

Under compressive stress, the cuts close while they open under tensile stress. Thus the closed-form expressions of the longitudinal Young's modulus E_1, under different stress conditions for Configuration 2 considering only beam-level bending deformation, are given as

$$E_1^C = \left(\frac{t}{l}\right)^3 \frac{E\cos\theta}{\left(\frac{h}{l}+\sin\theta\right)\sin^2\theta} \tag{94}$$

$$E_1^T = \left(\frac{t}{l}\right)^3 \frac{E(1-\alpha)^3\cos\theta}{\left(\frac{h}{l}+\sin\theta\right)\sin^2\theta} \tag{95}$$

The ratio of longitudinal Young's modulus under application of tensile stress to that under application of compressive stress is obtained by using the expressions (95) and (94)

$$\frac{E_1^T}{E_1^C} = (1-\alpha)^3 \tag{96}$$

This ratio defines the degree of non-invariance of longitudinal Young's moduli under tension and compression, which depends on α.

The Young's Modulus along the application of compressive stress σ_1, considering bending, axial and shear deformations, is given by

$$\begin{aligned} E_1^C &= \frac{\sigma_1}{\epsilon_1} \\ &= \left(\frac{t}{l}\right) \frac{E\cos\theta}{\left(\frac{h}{l}+\sin\theta\right)\sin^2\theta\left(\left(\frac{l}{t}\right)^2+\frac{2(1+\nu)}{k}+\cot^2\theta\right)} \end{aligned} \tag{97}$$

By a similar approach, the Young's modulus under the application of a uniform tensile stress, considering bending, axial and shear deformations, which causes the cuts to open is obtained by substituting thickness t by $t(1-\alpha)$ (where α gives the invariance effect) in the above equation, i.e.,

$$\begin{aligned} E_1^T &= \frac{\sigma_1}{\epsilon_1} \\ &= \left(\frac{t}{l}\right) \frac{E(1-\alpha)\cos\theta}{\left(\frac{h}{l}+\sin\theta\right)\sin^2\theta\left(\left(\frac{l}{t(1-\alpha)}\right)^2+\frac{2(1+\nu)}{k}+\cot^2\theta\right)} \end{aligned} \tag{98}$$

The ratio of longitudinal Young's modulus under application of tensile stress to that under application of compressive stress, considering bending, axial and shear deformation, is obtained by using the expressions (98) and (97)

$$\frac{E_1^T}{E_1^C} = \frac{(1-\alpha)\left(\left(\frac{l}{t}\right)^2+\frac{2(1+\nu)}{k}+\cot^2\theta\right)}{\left(\frac{l}{t(1-\alpha)}\right)^2+\frac{2(1+\nu)}{k}+\cot^2\theta} \tag{99}$$

This ratio defines the degree of non-invariance of longitudinal Young's moduli under tension and compression, which depends on α.

2.2.2. Poisson's ratio ν_{12}

The Poisson's ratio ν_{12} under only beam-level bending deformation is given as

$$\nu_{12} = \frac{\cos^2\theta}{\left(\frac{h}{l} + \sin\theta\right)\sin\theta} \tag{100}$$

Since Eq. (100) is the ratio of strains in two directions, it is identical under either compressive or tensile stress (i.e. degree of non-invariance for ν_{12} is 1).

Considering bending, axial and shear deformations, the Poisson's ratio ν_{12} under compressive far-field stress is given as

$$\nu_{12}^{C} = \frac{\cos^2\theta\left(\left(\frac{l}{t}\right)^2 + \frac{2(1+\nu)}{k} - 1\right)}{\left(\frac{h}{l} + \sin\theta\right)\sin\theta\left(\left(\frac{l}{t}\right)^2 + \frac{2(1+\nu)}{k} + \cot^2\theta\right)} \tag{101}$$

When tensile far-field stress is applied along direction-1, the cuts open and the Poisson's ratio ν_{12}, considering bending, axial and shear deformations, is obtained by replacing t with $t(1-\alpha)$ in the equation for ν_{12}^{C} above

$$\nu_{12}^{T} = \frac{\cos^2\theta\left(\left(\frac{l}{t(1-\alpha)}\right)^2 + \frac{2(1+\nu)}{k} - 1\right)}{\left(\frac{h}{l} + \sin\theta\right)\sin\theta\left(\left(\frac{l}{t(1-\alpha)}\right)^2 + \frac{2(1+\nu)}{k} + \cot^2\theta\right)} \tag{102}$$

Thus we see that under the effect of tensile stress, the Poisson's ratio ν_{12} is a function of α while under compressive stress, it is independent of α. The ratio of longitudinal Poisson's ratio under application of tensile stress to that under application of compressive stress, considering bending, axial and shear deformation, is obtained by using the expressions (102) and (101)

$$\frac{\nu_{12}^{T}}{\nu_{12}^{C}} = \frac{\left(\left(\frac{l}{t(1-\alpha)}\right)^2 + \frac{2(1+\nu)}{k} - 1\right)\left(\left(\frac{l}{t}\right)^2 + \frac{2(1+\nu)}{k} + \cot^2\theta\right)}{\left(\left(\frac{l}{t}\right)^2 + \frac{2(1+\nu)}{k} - 1\right)\left(\left(\frac{l}{t(1-\alpha)}\right)^2 + \frac{2(1+\nu)}{k} + \cot^2\theta\right)} \tag{103}$$

This ratio defines the degree of non-invariance of longitudinal Poisson's ratio under tension and compression, which depends on α.

2.2.3. Transverse Young's modulus E_2

Under compressive stress, the cuts open while they close under tensile stress. Thus the closed-form expressions of the transverse Young's modulus E_2, under different stress conditions considering only beam-level bending deformation, are given as

$$E_2^{C} = \left(\frac{t}{l}\right)^3 \frac{E\left(\frac{h}{l} + \sin\theta\right)(1-\alpha)^3}{\cos^3\theta} \tag{104}$$

$$E_2^{T} = \left(\frac{t}{l}\right)^3 \frac{E\left(\frac{h}{l} + \sin\theta\right)}{\cos^3\theta} \tag{105}$$

The ratio of transverse Young's modulus under application of tensile stress to that under application of compressive stress is obtained by using the expressions (105) and (104)

$$\frac{E_2^{T}}{E_2^{C}} = \frac{1}{(1-\alpha)^3} \tag{106}$$

This ratio defines the degree of non-invariance of transverse Young's moduli under tension and compression, which depends on α.

The Young's modulus along the application of compressive stress σ_2, considering bending, axial and shear deformations is given by

$$E_2^{C} = \left(\frac{t}{l}\right)\frac{E\left(\frac{h}{l} + \sin\theta\right)(1-\alpha)}{\cos^3\theta\left(\left(\frac{l}{t(1-\alpha)}\right)^2 + \frac{2(1+\nu)}{k} + \tan^2\theta + \frac{2}{\cos^2\theta}\left(\frac{h(1-\alpha)}{l}\right)\right)} \tag{107}$$

Under the application of tensile stress, the Young's modulus considering bending, axial and shear deformations is given by

$$E_2^{T} = \left(\frac{t}{l}\right)\frac{E\left(\frac{h}{l} + \sin\theta\right)}{\cos^3\theta\left(\left(\frac{l}{t}\right)^2 + \frac{2(1+\nu)}{k} + \tan^2\theta + \frac{2}{\cos^2\theta}\left(\frac{h}{l(1-\alpha)}\right)\right)} \tag{108}$$

The ratio of transverse Young's modulus under application of tensile stress to that under application of compressive stress, considering bending, axial and shear deformation, is obtained by using the expressions (108) and (107)

$$\frac{E_2^{T}}{E_2^{C}} = \frac{\left(\frac{l}{t(1-\alpha)}\right)^2 + \frac{2(1+\nu)}{k} + \tan^2\theta + \frac{2}{\cos^2\theta}\left(\frac{h}{l}\right)}{(1-\alpha)\left(\left(\frac{l}{t}\right)^2 + \frac{2(1+\nu)}{k} + \tan^2\theta + \frac{2}{\cos^2\theta}\left(\frac{h}{l}\right)\right)} \tag{109}$$

This ratio defines the degree of non-invariance of transverse Young's moduli under tension and compression, which depends on α.

2.2.4. Poisson's ratio ν_{21}

The Poisson's ratio ν_{21} considering only beam-level bending deformation is given as

$$\nu_{21} = \frac{\left(\frac{h}{l} + \sin\theta\right)\sin\theta}{\cos^2\theta} \tag{110}$$

Since Eq. (110) is the ratio of strains in two directions, it is identical under either compressive or tensile stress (i.e. degree of non-invariance for ν_{21} is 1).

Considering bending, axial and shear deformations, the Poisson's ratio ν_{21} under compressive stress is given as

$$\nu_{21}^{C} = \frac{\sin\theta\left(\frac{h}{l} + \sin\theta\right)\left(\left(\frac{l}{t(1-\alpha)}\right)^2 + \frac{2(1+\nu)}{k} - 1\right)}{\cos^2\theta\left(\left(\frac{l}{t(1-\alpha)}\right)^2 + \frac{2(1+\nu)}{k} + \tan^2\theta + \frac{2}{\cos^2\theta}\left(\frac{h(1-\alpha)}{l}\right)\right)} \tag{111}$$

When tensile stress is applied, the cuts open and the Poisson's ratio ν_{21}, considering bending, axial and shear deformations, is given by

$$\nu_{21}^{T} = \frac{\sin\theta\left(\frac{h}{l} + \sin\theta\right)\left(\left(\frac{l}{t}\right)^2 + \frac{2(1+\nu)}{k} - 1\right)}{\cos^2\theta\left(\left(\frac{l}{t}\right)^2 + \frac{2(1+\nu)}{k} + \tan^2\theta + \frac{2}{\cos^2\theta}\left(\frac{h}{l(1-\alpha)}\right)\right)} \tag{112}$$

Thus we see that under the effect of both compressive as well as tensile stress, the Poisson's ratio ν_{21} is a function of α. The ratio of transverse Poisson's ratio under application of tensile stress to that under application of compressive stress, considering bending, axial and shear deformation, is obtained by using the expressions (112) and (111)

$$\frac{\nu_{21}^{T}}{\nu_{21}^{C}} = \frac{\left(\left(\frac{l}{t}\right)^2 + \frac{2(1+\nu)}{k} - 1\right)\left(\left(\frac{l}{t(1-\alpha)}\right)^2 + \frac{2(1+\nu)}{k} + \tan^2\theta + \frac{2}{\cos^2\theta}\left(\frac{h(1-\alpha)}{l}\right)\right)}{\left(\left(\frac{l}{t(1-\alpha)}\right)^2 + \frac{2(1+\nu)}{k} - 1\right)\left(\left(\frac{l}{t}\right)^2 + \frac{2(1+\nu)}{k} + \tan^2\theta + \frac{2}{\cos^2\theta}\left(\frac{h}{l(1-\alpha)}\right)\right)} \tag{113}$$

This ratio defines the degree of non-invariance of transverse Poisson's ratio under tension and compression, which depends on α.

2.2.5. Shear modulus G_{12}

For configuration 2, the cuts in the vertical member BD as well as the inclined member BC close while those in the slant member AB open. Thus the shear modulus (under anticlockwise stress) considering only beam-level bending deformation is given by

$$G_{12}^{-} = \left(\frac{t}{l}\right)^3 \frac{E\left(\frac{h}{l} + \sin\theta\right)}{2\cos\theta\left(\frac{h}{l}\right)^2\left(\frac{1}{1+(1-\alpha)^3} + \frac{h}{l}\right)} \tag{114}$$

Now, we consider the case when the direction of the shear stress reverses (under clockwise stress). The cuts then fall on the convex side of the deformed member BD and thus open up. The quantification of shear modulus, G_{12}^{+}, is similar to as done above, except that in this case, the cuts in the vertical member BD as well as the inclined member BC open while those in the slant member AB close. Thus the shear modulus is given by

$$G_{12}^{+} = \left(\frac{t}{l}\right)^3 \frac{E\left(\frac{h}{l} + \sin\theta\right)}{2\cos\theta\left(\frac{h}{l}\right)^2\left(\frac{1}{1+(1-\alpha)^3} + \frac{h}{l(1-\alpha)^3}\right)} \tag{115}$$

The ratio of shear modulus under application of clockwise shear stress to that under application of anticlockwise shear stress is obtained by using the expressions (115) and (114)

$$\frac{G_{12}^{+}}{G_{12}^{-}} = \frac{\left(\frac{1}{1+(1-\alpha)^3} + \frac{h}{l}\right)}{\left(\frac{1}{1+(1-\alpha)^3} + \frac{h}{l(1-\alpha)^3}\right)} \tag{116}$$

This ratio defines the degree of non-invariance of shear moduli under clockwise and anticlockwise shear stress, which depends on α.

The shear modulus, considering beam-level bending, axial and shear deformations, under anti-clockwise shear stress, is given by

$$G_{12}^{-} = \frac{Eg_t}{2\cos\theta\left(\begin{array}{l}\left(\frac{g_h^2\left(1+\Phi_l(1-\alpha)^2\right)}{g_t^2(1-\alpha)^3\left(g_h+\sin\theta\right)} + g_h\left(1+\frac{\cos\theta\cot\theta}{\left(g_h+\sin\theta\right)}\right)\left(\frac{\alpha}{(\alpha-1)}\right)\right)\frac{1}{\left(1+\frac{1+\Phi_l(1-\alpha)^2}{\left(1+\Phi_l\right)(1-\alpha)^3}\right)} \\ +\frac{3g_h^3}{g_t^2\left(g_h+\sin\theta\right)}\left(\frac{1+\Phi_h}{12-\frac{36}{4+\Phi_h}}\right) + \frac{\sin\theta}{2}\left(\frac{2-\alpha}{1-\alpha}\right) + \left(\frac{1}{2}\tan^2\theta\left(g_h+\sin\theta\right)\left(\frac{2-\alpha}{1-\alpha}\right)\right) \\ +\frac{1}{2}\left(1+\frac{\cos\theta\cot\theta}{\left(g_h+\sin\theta\right)}\right)\left(g_h\left(\frac{\alpha}{\alpha-1}\right)+\sin\theta\left(\frac{2-\alpha}{1-\alpha}\right)\right)\end{array}\right)} \tag{117}$$

Similarly, when the direction of shear stress is reversed, the cuts BC and BD, as they come under tension open, while that of AB close. The shear modulus, considering beam-level bending, axial and shear deformations, under clockwise shear stress, is then given by

$$G_{12}^{+}=\frac{Eg_t}{2\cos\theta\left(\begin{array}{c}\left(\frac{g_h^2\left(1+\Phi_l\right)}{g_t^2\left(g_h+\sin\theta\right)}+g_h\left(1+\frac{\cos\theta\cot\theta}{\left(g_h+\sin\theta\right)}\right)\left(\frac{\alpha}{(1-\alpha)}\right)\right)\frac{1}{\left(1+\frac{\left(1+\Phi_l\right)(1-\alpha)^3}{1+\Phi_l(1-\alpha)^2}\right)}\\+\frac{3g_h^3}{g_t^2(1-\alpha)^3\left(g_h+\sin\theta\right)}\left(\frac{1+\Phi_h(1-\alpha)^2}{12-\frac{36}{4+\Phi_h(1-\alpha)^2}}\right)+\frac{\sin\theta}{2}\left(\frac{2-\alpha}{1-\alpha}\right)+\left(\tan^2\theta\left(g_h+\sin\theta\right)\right)\\+\frac{1}{2}\left(1+\frac{\cos\theta\cot\theta}{\left(g_h+\sin\theta\right)}\right)\left(g_h\left(\frac{\alpha}{(\alpha-1)}\right)+\sin\theta\left(\frac{2-\alpha}{1-\alpha}\right)\right)\end{array}\right)} \tag{118}$$

The ratio of Shear modulus under application of clockwise shear stress to that under application of anticlockwise shear stress is obtained by using the expressions (118) and (117)

$$\frac{G_{12}^{+}}{G_{12}^{-}}=\frac{\left(\begin{array}{c}\left(\frac{g_h^2\left(1+\Phi_l(1-\alpha)^2\right)}{g_t^2(1-\alpha)^3\left(g_h+\sin\theta\right)}+g_h\left(1+\frac{\cos\theta\cot\theta}{\left(g_h+\sin\theta\right)}\right)\left(\frac{\alpha}{(\alpha-1)}\right)\right)\frac{1}{\left(1+\frac{1+\Phi_l(1-\alpha)^2}{\left(1+\Phi_l\right)(1-\alpha)^3}\right)}\\+\frac{3g_h^3}{g_t^2\left(g_h+\sin\theta\right)}\left(\frac{1+\Phi_h}{12-\frac{36}{4+\Phi_h}}\right)+\frac{\sin\theta}{2}\left(\frac{2-\alpha}{1-\alpha}\right)+\left(\frac{1}{2}\tan^2\theta\left(g_h+\sin\theta\right)\left(\frac{2-\alpha}{1-\alpha}\right)\right)\\+\frac{1}{2}\left(1+\frac{\cos\theta\cot\theta}{\left(g_h+\sin\theta\right)}\right)\left(g_h\left(\frac{\alpha}{\alpha-1}\right)+\sin\theta\left(\frac{2-\alpha}{1-\alpha}\right)\right)\end{array}\right)}{\left(\begin{array}{c}\left(\frac{g_h^2\left(1+\Phi_l\right)}{g_t^2\left(g_h+\sin\theta\right)}+g_h\left(1+\frac{\cos\theta\cot\theta}{\left(g_h+\sin\theta\right)}\right)\left(\frac{\alpha}{(1-\alpha)}\right)\right)\frac{1}{\left(1+\frac{\left(1+\Phi_l\right)(1-\alpha)^3}{1+\Phi_l(1-\alpha)^2}\right)}\\+\frac{3g_h^3}{g_t^2(1-\alpha)^3\left(g_h+\sin\theta\right)}\left(\frac{1+\Phi_h(1-\alpha)^2}{12-\frac{36}{4+\Phi_h(1-\alpha)^2}}\right)+\frac{\sin\theta}{2}\left(\frac{2-\alpha}{1-\alpha}\right)+\left(\tan^2\theta\left(g_h+\sin\theta\right)\right)\\+\frac{1}{2}\left(1+\frac{\cos\theta\cot\theta}{\left(g_h+\sin\theta\right)}\right)\left(g_h\left(\frac{\alpha}{(\alpha-1)}\right)+\sin\theta\left(\frac{2-\alpha}{1-\alpha}\right)\right)\end{array}\right)} \tag{119}$$

This ratio defines the degree of non-invariance of shear moduli under clockwise and anticlockwise shear stress, which depends on α.

2.3. Critical remarks

2.3.1. Remark 1: Elastic moduli considering bending and axial deformations

For thin cell walls that are axially non-rigid, the axial deformation needs to be accounted for in addition to the bending deformation. Thus the expression of the elastic moduli are obtained by neglecting beam-level shear deformation components of Equations (46), (47), (51), (52), (60), (67), (71), (72), (90) and (92) for configuration 1.

$$E_1^C=\left(\frac{t}{l}\right)\frac{E(1-\alpha)\cos\theta}{\left(\frac{h}{l}+\sin\theta\right)\sin^2\theta\left(\left(\frac{l}{t(1-\alpha)}\right)^2+\cot^2\theta\right)} \tag{120}$$

$$E_1^T=\left(\frac{t}{l}\right)\frac{E\cos\theta}{\left(\frac{h}{l}+\sin\theta\right)\sin^2\theta\left(\left(\frac{l}{t}\right)^2+\cot^2\theta\right)} \tag{121}$$

$$\nu_{12}^C=\frac{\cos^2\theta\left(\left(\frac{l}{t(1-\alpha)}\right)^2-1\right)}{\left(\frac{h}{l}+\sin\theta\right)\sin\theta\left(\left(\frac{l}{t(1-\alpha)}\right)^2+\cot^2\theta\right)} \tag{122}$$

$$\nu_{12}^T=\frac{\cos^2\theta\left(\left(\frac{l}{t}\right)^2-1\right)}{\left(\frac{h}{l}+\sin\theta\right)\sin\theta\left(\left(\frac{l}{t}\right)^2+\cot^2\theta\right)} \tag{123}$$

$$E_2^C=\left(\frac{t}{l}\right)\frac{E\left(\frac{h}{l}+\sin\theta\right)}{\cos^3\theta\left(\left(\frac{l}{t}\right)^2+\tan^2\theta+\frac{2}{\cos^2\theta}\left(\frac{h}{l}\right)\right)} \tag{124}$$

$$E_2^T = \left(\frac{t}{l}\right)\frac{E\left(\frac{h}{l}+\sin\theta\right)(1-\alpha)}{\cos^3\theta\left(\left(\frac{l}{t(1-\alpha)}\right)^2+\tan^2\theta+\frac{2}{\cos^2\theta}\left(\frac{h}{l}\right)\right)} \tag{125}$$

$$\nu_{21}^C = \frac{\sin\theta\left(\frac{h}{l}+\sin\theta\right)\left(\left(\frac{l}{t}\right)^2-1\right)}{\cos^2\theta\left(\left(\frac{l}{t}\right)^2+\tan^2\theta+\frac{2}{\cos^2\theta}\left(\frac{h}{l}\right)\right)} \tag{126}$$

$$\nu_{21}^T = \frac{\sin\theta\left(\frac{h}{l}+\sin\theta\right)\left(\left(\frac{l}{t(1-\alpha)}\right)^2-1\right)}{\cos^2\theta\left(\left(\frac{l}{t(1-\alpha)}\right)^2+\tan^2\theta+\frac{2}{\cos^2\theta}\left(\frac{h}{l}\right)\right)} \tag{127}$$

$$G_{12}^- = \frac{Eg_t}{2\cos\theta\left(\begin{array}{c}\left(\frac{g_h^2}{g_t^2\left(g_h+\sin\theta\right)}+g_h\left(1+\frac{\cos\theta\cot\theta}{\left(g_h+\sin\theta\right)}\right)\left(\frac{\alpha}{1-\alpha}\right)\right)\frac{1}{\left(1+(1-\alpha)^3\right)}\\ +\frac{g_h^3}{g_t^2(1-\alpha)^3\left(g_h+\sin\theta\right)}+\frac{\sin\theta}{2}\left(\frac{2-\alpha}{1-\alpha}\right)+\left(\tan^2\theta\left(g_h+\sin\theta\right)\right)\\ +\frac{1}{2}\left(1+\frac{\cos\theta\cot\theta}{\left(g_h+\sin\theta\right)}\right)\left(g_h\left(\frac{\alpha}{\alpha-1}\right)+\sin\theta\left(\frac{2-\alpha}{1-\alpha}\right)\right)\end{array}\right)} \tag{128}$$

$$G_{12}^+ = \frac{Eg_t}{2\cos\theta\left(\begin{array}{c}\left(\frac{g_h^2}{g_t^2(1-\alpha)^3\left(g_h+\sin\theta\right)}+g_h\left(1+\frac{\cos\theta\cot\theta}{\left(g_h+\sin\theta\right)}\right)\left(\frac{\alpha}{\alpha-1}\right)\right)\frac{1}{\left(1+\frac{1}{(1-\alpha)^3}\right)}\\ +\frac{g_h^3}{g_t^2\left(g_h+\sin\theta\right)}+\frac{\sin\theta}{2}\left(\frac{2-\alpha}{1-\alpha}\right)+\left(\frac{1}{2}\tan^2\theta\left(g_h+\sin\theta\right)\left(\frac{2-\alpha}{1-\alpha}\right)\right)\\ +\frac{1}{2}\left(1+\frac{\cos\theta\cot\theta}{\left(g_h+\sin\theta\right)}\right)\left(g_h\left(\frac{\alpha}{1-\alpha}\right)+\sin\theta\left(\frac{2-\alpha}{1-\alpha}\right)\right)\end{array}\right)} \tag{129}$$

Note that the expressions corresponding to the Configuration 2 are presented in the supplementary section 1.1.

2.3.2. Remark 2: Elastic moduli considering bending and shear deformations

For thick cell walls that are axially rigid, the beam-level shear deformation needs to be accounted for in addition to the bending deformation. Thus the expression of the elastic moduli are obtained by considering axial deformation components of Equations (46), (47), (51), (52), (60), (67), (71), (72), (90) and (92) for configuration 1 to vanish.

$$E_1^C = \left(\frac{t}{l}\right)\frac{E(1-\alpha)\cos\theta}{\left(\frac{h}{l}+\sin\theta\right)\sin^2\theta\left(\left(\frac{l}{t(1-\alpha)}\right)^2+\frac{2(1+\nu)}{k}\right)} \tag{130}$$

$$E_1^T = \left(\frac{t}{l}\right)\frac{E\cos\theta}{\left(\frac{h}{l}+\sin\theta\right)\sin^2\theta\left(\left(\frac{l}{t}\right)^2+\frac{2(1+\nu)}{k}\right)} \tag{131}$$

$$\nu_{12}^C = \frac{\cos^2\theta}{\left(\frac{h}{l}+\sin\theta\right)\sin\theta} \tag{132}$$

$$\nu_{12}^T = \frac{\cos^2\theta}{\left(\frac{h}{l}+\sin\theta\right)\sin\theta} \tag{133}$$

$$E_2^C = \left(\frac{t}{l}\right)\frac{E\left(\frac{h}{l}+\sin\theta\right)}{\cos^3\theta\left(\left(\frac{l}{t}\right)^2+\frac{2(1+\nu)}{k}\right)} \tag{134}$$

$$E_2^T = \left(\frac{t}{l}\right)\frac{E\left(\frac{h}{l}+\sin\theta\right)(1-\alpha)}{\cos^3\theta\left(\left(\frac{l}{t(1-\alpha)}\right)^2+\frac{2(1+\nu)}{k}\right)} \tag{135}$$

$$\nu_{21}^C = \frac{\sin\theta\left(\frac{h}{l}+\sin\theta\right)}{\cos^2\theta} \tag{136}$$

$$\nu_{21}^T = \frac{\sin\theta\left(\frac{h}{l}+\sin\theta\right)}{\cos^2\theta} \tag{137}$$

$$G_{12}^{-}=\frac{Eg_t}{2\cos\theta\left(\begin{array}{l}\left(\dfrac{g_h^2\left(1+\Phi_l\right)}{g_t^2\left(g_h+\sin\theta\right)}\right)\dfrac{1}{\left(1+\dfrac{\left(1+\Phi_l\right)(1-\alpha)^3}{1+\Phi_l(1-\alpha)^2}\right)}\\+\dfrac{3g_h^3}{g_t^2(1-\alpha)^3\left(g_h+\sin\theta\right)}\left(\dfrac{1+\Phi_h(1-\alpha)^2}{12-\dfrac{36}{4+\Phi_h(1-\alpha)^2}}\right)\end{array}\right)} \tag{138}$$

$$G_{12}^{+}=\frac{Eg_t}{2\cos\theta\left(\begin{array}{l}\left(\dfrac{g_h^2\left(1+\Phi_l(1-\alpha)^2\right)}{g_t^2(1-\alpha)^3\left(g_h+\sin\theta\right)}\right)\dfrac{1}{\left(1+\dfrac{1+\Phi_l(1-\alpha)^2}{\left(1+\Phi_l\right)(1-\alpha)^3}\right)}\\+\dfrac{3g_h^3}{g_t^2\left(g_h+\sin\theta\right)}\left(\dfrac{1+\Phi_h}{12-\dfrac{36}{4+\Phi_h}}\right)\end{array}\right)} \tag{139}$$

Note here that the Poisson's ratios (ν_{12} and ν_{21}) are equal for both compressive and tensile mode of stresses. The expressions corresponding to the Configuration 2 are presented in the supplementary section 1.2.

2.3.3. Remark 3: Applicability to differently shaped lattices

The five elastic constants derived for hexagonal honeycomb lattices with cuts can be applied to other lattices with different shapes, as shown in Fig. 1(C–E). Such shapes of the lattices result from the appropriate change in the geometry of the hexagonal lattices (i.e. slight modifications need to be introduced in the expressions (46), (47), (51), (52), (60), (67), (71), (72), (90) and (92)).

Consider the re-entrant auxetic lattices for instance (refer to Fig. 1(B(ii) and C)). The effective elastic constants of such lattices can be easily obtained by changing θ to $-\theta$ in the equations (46), (47), (51), (52), (60), (67), (71), (72), (90) and (92). This derivation is quite straightforward; thus, here the final expressions for lattices with negative Poisson's ratio is not shown. However, we have presented the numerical results for auxetic configurations in this article later.

Following a similar approach, elastic constants of rectangular lattices (as shown in Fig. 1(B(iii) and D)) can be obtained by taking limit $\theta \to 0$.

$$E_1^C=\lim_{\theta\to0}\left(\frac{t}{l}\right)\frac{E(1-\alpha)\cos\theta}{\left(\frac{h}{l}+\sin\theta\right)\sin^2\theta\left(\left(\frac{l}{t(1-\alpha)}\right)^2+\frac{2(1+\nu)}{k}+\cot^2\theta\right)}=\frac{Et(1-\alpha)}{h} \tag{140}$$

$$E_1^T=\lim_{\theta\to0}\left(\frac{t}{l}\right)\frac{E\cos\theta}{\left(\frac{h}{l}+\sin\theta\right)\sin^2\theta\left(\left(\frac{l}{t}\right)^2+\frac{2(1+\nu)}{k}+\cot^2\theta\right)}=\frac{Et}{h} \tag{141}$$

$$\nu_{12}^C=\lim_{\theta\to0}\frac{\cos^2\theta\left(\left(\frac{l}{t(1-\alpha)}\right)^2+\frac{2(1+\nu)}{k}-1\right)}{\left(\frac{h}{l}+\sin\theta\right)\sin\theta\left(\left(\frac{l}{t(1-\alpha)}\right)^2+\frac{2(1+\nu)}{k}+\cot^2\theta\right)}=0 \tag{142}$$

$$\nu_{12}^T=\lim_{\theta\to0}\frac{\cos^2\theta\left(\left(\frac{l}{t}\right)^2+\frac{2(1+\nu)}{k}-1\right)}{\left(\frac{h}{l}+\sin\theta\right)\sin\theta\left(\left(\frac{l}{t}\right)^2+\frac{2(1+\nu)}{k}+\cot^2\theta\right)}=0 \tag{143}$$

$$\begin{aligned}E_2^C&=\lim_{\theta\to0}\left(\frac{t}{l}\right)\frac{E\left(\frac{h}{l}+\sin\theta\right)}{\cos^3\theta\left(\left(\frac{l}{t}\right)^2+\frac{2(1+\nu)}{k}+\tan^2\theta+\frac{2}{\cos^2\theta}\left(\frac{h}{l}\right)\right)}\\&=\left(\frac{t}{l}\right)\frac{E\left(\frac{h}{l}\right)}{\left(\left(\frac{l}{t}\right)^2+\frac{2(1+\nu)}{k}+\left(\frac{2h}{l}\right)\right)}\end{aligned} \tag{144}$$

$$\begin{aligned}E_2^T&=\lim_{\theta\to0}\left(\frac{t}{l}\right)\frac{E\left(\frac{h}{l}+\sin\theta\right)(1-\alpha)}{\cos^3\theta\left(\left(\frac{l}{t(1-\alpha)}\right)^2+\frac{2(1+\nu)}{k}+\tan^2\theta+\frac{2}{\cos^2\theta}\left(\frac{h}{l}\right)\right)}\\&=\left(\frac{t}{l}\right)\frac{E\left(\frac{h}{l}\right)(1-\alpha)}{\left(\left(\frac{l}{t(1-\alpha)}\right)^2+\frac{2(1+\nu)}{k}+\left(\frac{2h}{l}\right)\right)}\end{aligned} \tag{145}$$

$$\nu_{21}^{C} = \lim_{\theta\to 0} \frac{\sin\theta\left(\frac{h}{l}+\sin\theta\right)\left(\left(\frac{l}{t}\right)^2+\frac{2(1+\nu)}{k}-1\right)}{\cos^2\theta\left(\left(\frac{l}{t}\right)^2+\frac{2(1+\nu)}{k}+\tan^2\theta+\frac{2}{\cos^2\theta}\left(\frac{h}{l}\right)\right)} = 0 \tag{146}$$

$$\nu_{21}^{T} = \lim_{\theta\to 0} \frac{\sin\theta\left(\frac{h}{l}+\sin\theta\right)\left(\left(\frac{l}{t(1-\alpha)}\right)^2+\frac{2(1+\nu)}{k}-1\right)}{\cos^2\theta\left(\left(\frac{l}{t(1-\alpha)}\right)^2+\frac{2(1+\nu)}{k}+\tan^2\theta+\frac{2}{\cos^2\theta}\left(\frac{h}{l}\right)\right)} = 0 \tag{147}$$

In case of deriving the shear modulus of rectangular lattices, some physical facts become evident. For rectangular lattices, there will be no shear strain due to beam-level axial deformation as the axial forces on the slant members act along one line causing compression in one and tension in the other. The shear strain at the unit cell level arises from the beam-level bending and shear deformations. Thus for shear modulus of rectangular lattices, we have (from Equations (81) and (82))

$$\begin{aligned}\phi &= \lim_{\theta\to 0} \frac{Fhl\left(1+\frac{2(1+\nu)}{k}\left(\frac{t}{l}\right)^2\right)}{Ebt^3\left(1+\frac{\left(1+\frac{2(1+\nu)}{k}\left(\frac{t}{l}\right)^2\right)(1-\alpha)^3}{\left(1+\frac{2(1+\nu)}{k}\left(\frac{t(1-\alpha)}{l}\right)^2\right)}\right)} \\ &= \lim_{\theta\to 0} \frac{2\tau g_h\cos\theta\left(1+\Phi_l\right)}{Eg_t^3\left(\frac{\left(1+\Phi_l\right)\left(1-\alpha^3\right)}{1+\Phi_l(1-\alpha)^2}\right)} \\ &= \frac{2\tau g_h\left(1+\Phi_l\right)}{Eg_t^3\left(\frac{\left(1+\Phi_l\right)\left(1-\alpha^3\right)}{1+\Phi_l(1-\alpha)^2}\right)}\end{aligned} \tag{148}$$

$$\begin{aligned}\eta_D &= \lim_{\theta\to 0} \frac{12F\left(\frac{h}{2}\right)^3}{Ebt^3(1-\alpha)^3}\left(\frac{1+\frac{2(1+\nu)}{k}\left(\frac{2t(1-\alpha)}{h}\right)^2}{12-\frac{36}{4+\frac{2(1+\nu)}{k}\left(\frac{2t(1-\alpha)}{h}\right)^2}}\right) \\ &= \lim_{\theta\to 0} \frac{3\tau l\cos\theta g_h^3}{Eg_t^3(1-\alpha)^3}\left(\frac{1+\Phi_h(1-\alpha)^2}{12-\frac{36}{4+\Phi_h(1-\alpha)^2}}\right) \\ &= \frac{3\tau l g_h^3}{Eg_t^3(1-\alpha)^3}\left(\frac{1+\Phi_h(1-\alpha)^2}{12-\frac{36}{4+\Phi_h(1-\alpha)^2}}\right)\end{aligned} \tag{149}$$

Total shear strain for a rectangular lattice is thus give as

$$\begin{aligned}\gamma_t &= \frac{2\left(\phi\frac{h}{2}+\eta_D\right)}{h+l\sin\theta} \\ &= \frac{2\tau g_h^2\left(1+\Phi_l\right)}{Eg_t^3\left(\frac{\left(1+\Phi_l\right)\left(1-\alpha^3\right)}{1+\Phi_l(1-\alpha)^2}\right)\left(g_h+\sin\theta\right)} + \frac{6\tau g_h^3}{Eg_t^3\left(g_h+\sin\theta\right)(1-\alpha)^3}\left(\frac{1+\Phi_h(1-\alpha)^2}{12-\frac{36}{4+\Phi_h(1-\alpha)^2}}\right)\end{aligned} \tag{150}$$

The shear modulus (under anti-clockwise shear stress) is given as

$$\begin{aligned}G_{12}^{-} &= \frac{\tau}{\gamma_t} \\ &= \frac{Eg_t^3\left(g_h+\sin\theta\right)}{2g_h^2\left(\frac{\left(1+\Phi_l\right)}{\left(\frac{\left(1+\Phi_l\right)\left(1-\alpha^3\right)}{1+\Phi_l(1-\alpha)^2}\right)}+\frac{3g_h}{(1-\alpha)^3}\left(\frac{1+\Phi_h(1-\alpha)^2}{12-\frac{36}{4+\Phi_h(1-\alpha)^2}}\right)\right)}\end{aligned} \tag{151}$$

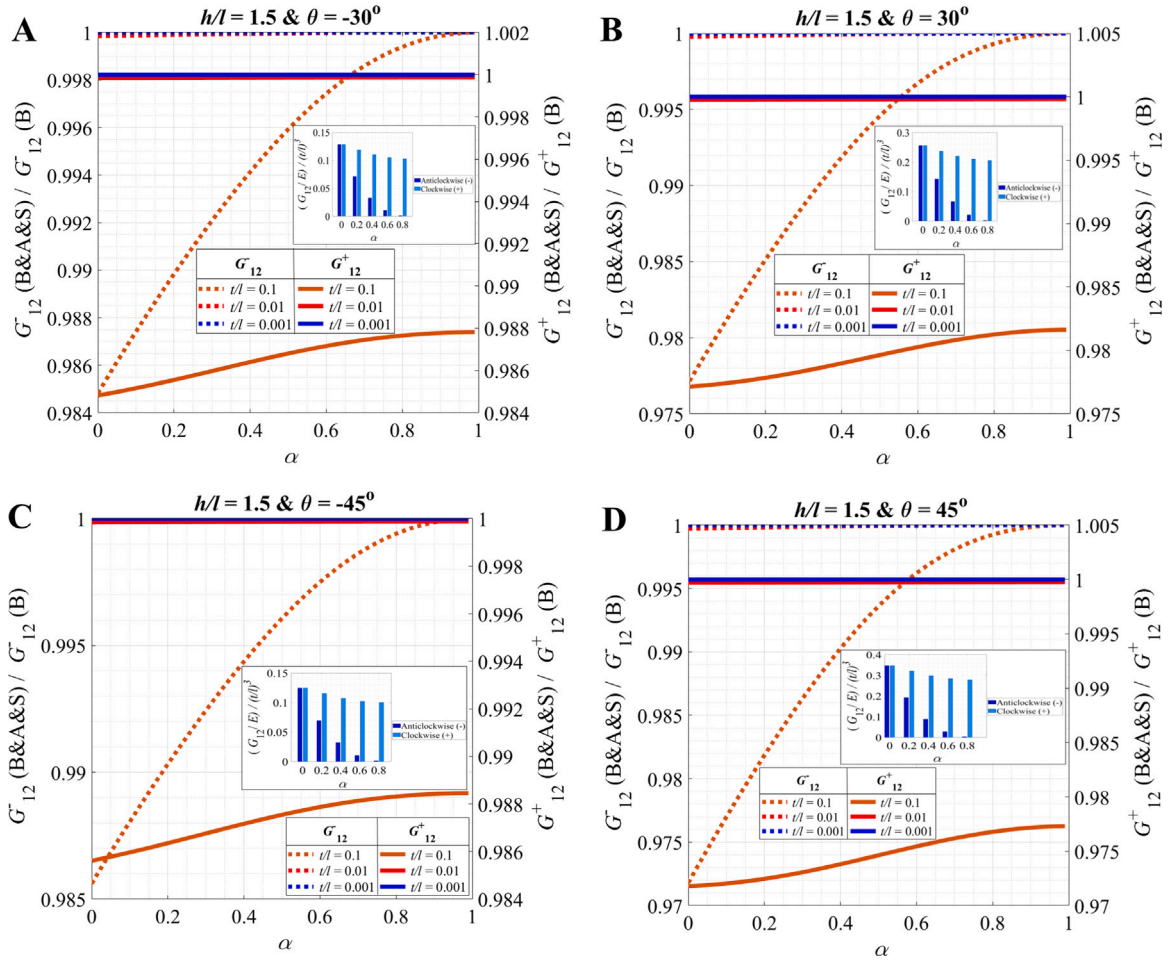

Fig. 10. Effect of beam-level shear and axial deformation on in-plane shear modulus. (A–D) Variation of ratio of shear modulus, considering bending, axial and shear deformations (denoted by B, A and S, respectively, in figure) to the shear modulus, considering only bending deformation with the ratio of depth of cut to total thickness of cell wall, α, for different auxetic and non-auxetic configurations. The figures in inset show the variation of non-dimensionalized shear modulus to α, considering only bending deformation, for the unit cell subjected to clockwise and anti-clockwise shear stresses. Note that the main plot here is intended to show the effect of beam-level axial and shear deformations with respect to only bending deformation. The inset plots give the variation trend of the shear modulus with α. In each of the subplots, the shear modulus is presented for clockwise and anti-clockwise modes of far-field shear stresses considering the Configuration 1 of domain discontinuity.

Similarly, the shear modulus of rectangular lattice on application of clockwise shear stress is given as

$$G_{12}^{+}=\frac{Eg_t^3\left(g_h+\sin\theta\right)}{2g_h^2\left(\left(\frac{\left(1+\Phi_l\left(1-\alpha\right)^2\right)}{\left(1-\alpha\right)^3}\right)\frac{1}{\left(1+\frac{1+\Phi_l\left(1-\alpha\right)^2}{\left(1+\Phi_l\right)\left(1-\alpha\right)^3}\right)}+3g_h\left(\frac{1+\Phi_h}{12-\frac{36}{4+\Phi_h}}\right)\right)} \tag{152}$$

If we instead take limit $h\to 0$, the elastic constants of rhombic lattices (refer to Fig. 1(B(iv) and E)) can be obtained as

$$\begin{aligned}E_1^C&=\lim_{h\to 0}\left(\frac{t}{l}\right)\frac{E\left(1-\alpha\right)\cos\theta}{\left(\frac{h}{l}+\sin\theta\right)\sin^2\theta\left(\left(\frac{l}{t\left(1-\alpha\right)}\right)^2+\frac{2\left(1+\nu\right)}{k}+\cot^2\theta\right)}\\&=\left(\frac{t}{l}\right)\frac{E\left(1-\alpha\right)\cos\theta}{\sin^3\theta\left(\left(\frac{l}{t\left(1-\alpha\right)}\right)^2+\frac{2\left(1+\nu\right)}{k}+\cot^2\theta\right)}\end{aligned} \tag{153}$$

$$\begin{aligned}E_1^T&=\lim_{h\to 0}\left(\frac{t}{l}\right)\frac{E\cos\theta}{\left(\frac{h}{l}+\sin\theta\right)\sin^2\theta\left(\left(\frac{l}{t}\right)^2+\frac{2\left(1+\nu\right)}{k}+\cot^2\theta\right)}\\&=\left(\frac{t}{l}\right)\frac{E\cos\theta}{\sin^3\theta\left(\left(\frac{l}{t}\right)^2+\frac{2\left(1+\nu\right)}{k}+\cot^2\theta\right)}\end{aligned} \tag{154}$$

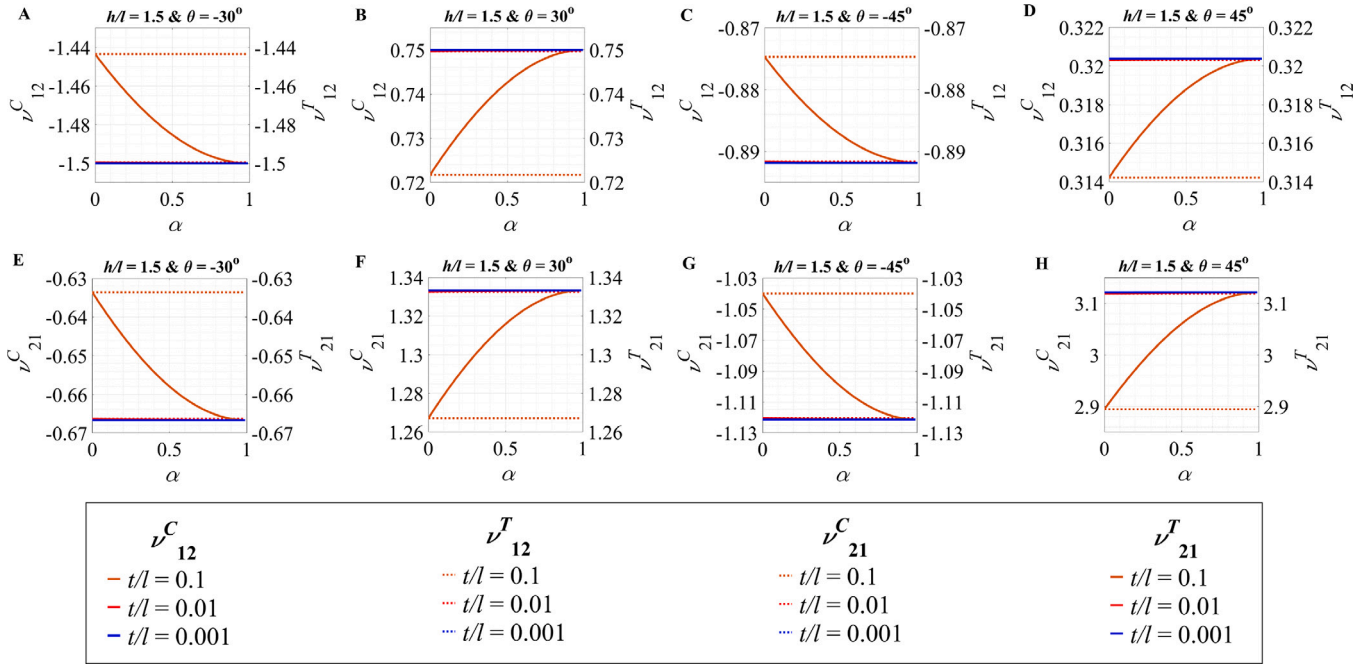

Fig. 11. Non-invariant in-plane Poisson's ratios considering beam-level bending, axial and shear deformations. (A–D) Variation of Poisson's ratio ν_{12}, considering bending, axial and shear deformations, with the ratio of depth of cut to total thickness of cell wall, α, for different auxetic and non-auxetic configurations. **(E–H)** Variation of Poisson's ratio ν_{21}, considering bending, axial and shear deformations, with the ratio of depth of cut to total thickness of cell wall, α, for different auxetic and non-auxetic configurations. In each of the subplots, the Poisson's ratios are presented for compressive and tensile modes of far-field stresses considering the Configuration 1 of domain discontinuity.

$$\nu_{12}^{C} = \lim_{h\to 0} \frac{\cos^2\theta\left(\left(\frac{l}{t(1-\alpha)}\right)^2 + \frac{2(1+\nu)}{k} - 1\right)}{\left(\frac{h}{l} + \sin\theta\right)\sin\theta\left(\left(\frac{l}{t(1-\alpha)}\right)^2 + \frac{2(1+\nu)}{k} + \cot^2\theta\right)} = \frac{\cos^2\theta\left(\left(\frac{l}{t(1-\alpha)}\right)^2 + \frac{2(1+\nu)}{k} - 1\right)}{\sin^2\theta\left(\left(\frac{l}{t(1-\alpha)}\right)^2 + \frac{2(1+\nu)}{k} + \cot^2\theta\right)} \tag{155}$$

$$\nu_{12}^{T} = \lim_{h\to 0} \frac{\cos^2\theta\left(\left(\frac{l}{t}\right)^2 + \frac{2(1+\nu)}{k} - 1\right)}{\left(\frac{h}{l} + \sin\theta\right)\sin\theta\left(\left(\frac{l}{t}\right)^2 + \frac{2(1+\nu)}{k} + \cot^2\theta\right)} = \frac{\cos^2\theta\left(\left(\frac{l}{t}\right)^2 + \frac{2(1+\nu)}{k} - 1\right)}{\sin^2\theta\left(\left(\frac{l}{t}\right)^2 + \frac{2(1+\nu)}{k} + \cot^2\theta\right)} \tag{156}$$

$$E_2^{C} = \lim_{h\to 0}\left(\frac{t}{l}\right)\frac{E\left(\frac{h}{l} + \sin\theta\right)}{\cos^3\theta\left(\left(\frac{l}{t}\right)^2 + \frac{2(1+\nu)}{k} + \tan^2\theta + \frac{2}{\cos^2\theta}\left(\frac{h}{l}\right)\right)} = \left(\frac{t}{l}\right)\frac{E\sin\theta}{\cos^3\theta\left(\left(\frac{l}{t}\right)^2 + \frac{2(1+\nu)}{k} + \tan^2\theta\right)} \tag{157}$$

$$E_2^{T} = \lim_{h\to 0}\left(\frac{t}{l}\right)\frac{E\left(\frac{h}{l} + \sin\theta\right)(1-\alpha)}{\cos^3\theta\left(\left(\frac{l}{t(1-\alpha)}\right)^2 + \frac{2(1+\nu)}{k} + \tan^2\theta + \frac{2}{\cos^2\theta}\left(\frac{h}{l}\right)\right)} = \left(\frac{t}{l}\right)\frac{E\sin\theta(1-\alpha)}{\cos^3\theta\left(\left(\frac{l}{t(1-\alpha)}\right)^2 + \frac{2(1+\nu)}{k} + \tan^2\theta\right)} \tag{158}$$

$$\nu_{21}^{C} = \lim_{h\to 0} \frac{\sin\theta\left(\frac{h}{l}+\sin\theta\right)\left(\left(\frac{l}{t}\right)^2+\frac{2(1+\nu)}{k}-1\right)}{\cos^2\theta\left(\left(\frac{l}{t}\right)^2+\frac{2(1+\nu)}{k}+\tan^2\theta+\frac{2}{\cos^2\theta}\left(\frac{h}{l}\right)\right)} = \frac{\sin^2\theta\left(\left(\frac{l}{t}\right)^2+\frac{2(1+\nu)}{k}-1\right)}{\cos^2\theta\left(\left(\frac{l}{t}\right)^2+\frac{2(1+\nu)}{k}+\tan^2\theta\right)} \tag{159}$$

$$\nu_{21}^{T} = \lim_{h\to 0} \frac{\sin\theta\left(\frac{h}{l}+\sin\theta\right)\left(\left(\frac{l}{t(1-\alpha)}\right)^2+\frac{2(1+\nu)}{k}-1\right)}{\cos^2\theta\left(\left(\frac{l}{t(1-\alpha)}\right)^2+\frac{2(1+\nu)}{k}+\tan^2\theta+\frac{2}{\cos^2\theta}\left(\frac{h}{l}\right)\right)} = \frac{\sin^2\theta\left(\left(\frac{l}{t(1-\alpha)}\right)^2+\frac{2(1+\nu)}{k}-1\right)}{\cos^2\theta\left(\left(\frac{l}{t(1-\alpha)}\right)^2+\frac{2(1+\nu)}{k}+\tan^2\theta\right)} \tag{160}$$

$$G_{12}^{-} = \lim_{h\to 0} \frac{Eg_t}{2\cos\theta\left(\begin{array}{l}\left(\frac{g_h^2\left(1+\Phi_l\right)}{g_t^2\left(g_h+\sin\theta\right)}+g_h\left(1+\frac{\cos\theta\cot\theta}{\left(g_h+\sin\theta\right)}\right)\left(\frac{\alpha}{(1-\alpha)}\right)\right)\frac{1}{\left(1+\frac{\left(1+\Phi_l\right)(1-\alpha)^3}{1+\Phi_l(1-\alpha)^2}\right)}\\ +\frac{3g_h^3}{g_t^2(1-\alpha)^3\left(g_h+\sin\theta\right)}\left(\frac{1+\Phi_h(1-\alpha)^2}{12-\frac{36}{4+\Phi_h(1-\alpha)^2}}\right)+\frac{\sin\theta}{2}\left(\frac{2-\alpha}{1-\alpha}\right)+\left(\tan^2\theta\left(g_h+\sin\theta\right)\right)\\ +\frac{1}{2}\left(1+\frac{\cos\theta\cot\theta}{\left(g_h+\sin\theta\right)}\right)\left(g_h\left(\frac{\alpha}{(\alpha-1)}\right)+\sin\theta\left(\frac{2-\alpha}{1-\alpha}\right)\right)\end{array}\right)} = \frac{Eg_t}{\sin\theta\cos\theta\left(\left(1+\csc^2\theta\right)\left(\frac{2-\alpha}{1-\alpha}\right)+2\tan^2\theta\right)} \tag{161}$$

$$G_{12}^{+} = \lim_{h\to 0} \frac{Eg_t}{2\cos\theta\left(\begin{array}{l}\left(\frac{g_h^2\left(1+\Phi_l(1-\alpha)^2\right)}{g_t^2(1-\alpha)^3\left(g_h+\sin\theta\right)}+g_h\left(1+\frac{\cos\theta\cot\theta}{\left(g_h+\sin\theta\right)}\right)\left(\frac{\alpha}{(\alpha-1)}\right)\right)\frac{1}{\left(1+\frac{1+\Phi_l(1-\alpha)^2}{\left(1+\Phi_l\right)(1-\alpha)^3}\right)}\\ +\frac{3g_h^3}{g_t^2\left(g_h+\sin\theta\right)}\left(\frac{1+\Phi_h}{12-\frac{36}{4+\Phi_h}}\right)+\frac{\sin\theta}{2}\left(\frac{2-\alpha}{1-\alpha}\right)+\left(\frac{1}{2}\tan^2\theta\left(g_h+\sin\theta\right)\left(\frac{2-\alpha}{1-\alpha}\right)\right)\\ +\frac{1}{2}\left(1+\frac{\cos\theta\cot\theta}{\left(g_h+\sin\theta\right)}\right)\left(g_h\left(\frac{\alpha}{\alpha-1}\right)+\sin\theta\left(\frac{2-\alpha}{1-\alpha}\right)\right)\end{array}\right)} = \frac{Eg_t\sin\theta\cos\theta(1-\alpha)}{(2-\alpha)} \tag{162}$$

Note that the expressions given above for differently shape lattices correspond to Configuration 1. The expressions for Configuration 2 are presented in the supplementary section 1.3.

3. Results and discussion

In this section, numerical results are presented in order to characterize the effect of introducing cuts (i.e. domain discontinuities) in lattice structures using the analytical expressions derived in the preceding section. It may be noted that the lattice-level effective elastic properties essentially depend on the beam-level deformation behavior. Thus, it is necessary to validate the expression of deflection of a beam with cuts introduced, under the boundary conditions for a cantilever beam with no rotation allowed at the free end (refer to Fig. 6(C)(i)). To do this validation, a cantilever beam is considered with the aforementioned boundary conditions and the results are compared for transverse deflection obtained based on beam-level theoretical derivation and finite element simulations using commercial codes (Anon, 2021). In the finite element simulation, we have modeled a 3D single solid block of length $l = 5$ mm, width $b = 2.5$ mm, and thickness $t = 1$ mm. Linear pattern tool is used to create 70 elements with no clearance between the patterns. The rest volume is extruded to obtain a total volume of 70 mm × 5 mm × 5 mm. The contact surfaces of the cuts are made frictional with varying frictional coefficients which will result in a difference in force needed to produce the same deflection in case of closing of cuts. In the case of opening as there will be no or minimal contact between cut surfaces, it may vary with negligible values. One end of the surface of the beam has been given a fixed support and the other end is given a remote displacement of 6 mm and rotations of the surfaces are restricted. Fig. 6 shows that increasing the friction coefficient results in a better match between theory and finite element analysis.

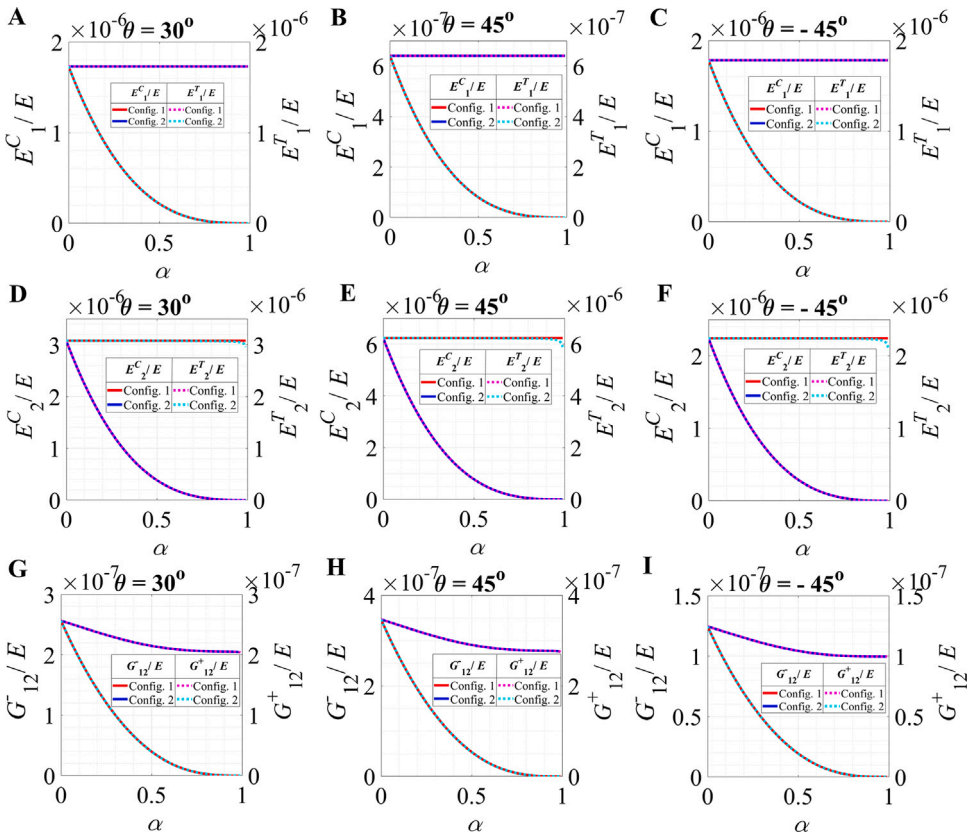

Fig. 12. Comparison of non-invariant in-plane Young's and shear moduli for Configuration 1 and 2 of hexagonal lattices considering beam-level bending, axial and shear deformations. (A–C) Variation of non-dimensionalized Young's modulus in longitudinal direction, i.e., E_1/E with the ratio of depth of cut to total thickness of cell wall, α, for different auxetic and non-auxetic combinations, for both Configuration 1 and Configuration 2. **(D–F)** Variation of non-dimensionalized Young's modulus in transverse direction, i.e., E_2/E with the ratio of depth of cut to total thickness of cell wall, α, for different auxetic and non-auxetic combinations, for both Configuration 1 and Configuration 2. **(G–I)** Variation of non-dimensionalized shear modulus, i.e., G_{12}/E with the ratio of depth of cut to total thickness of cell wall, α, for different auxetic and non-auxetic combinations, for both Configuration 1 and Configuration 2. Note that the figure is plotted considering the geometric parameter $h/l = 1.5$.

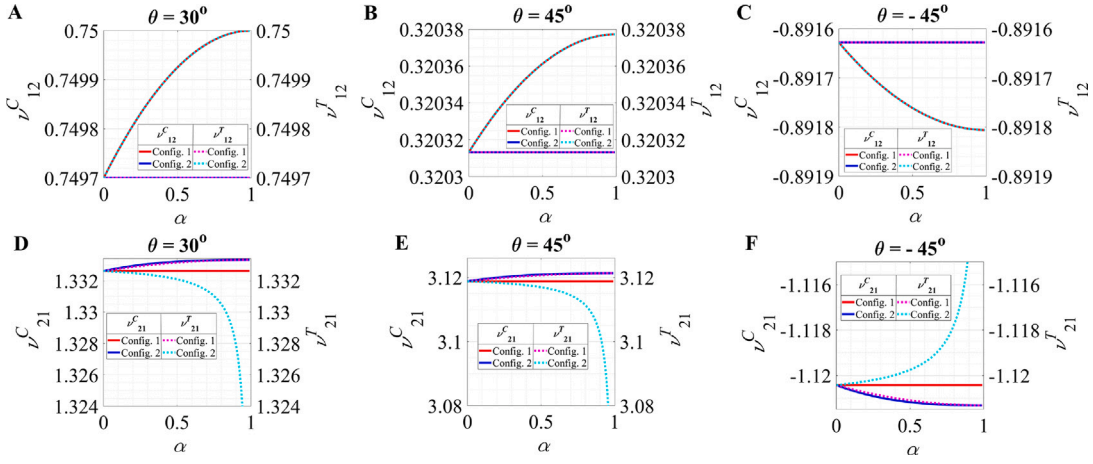

Fig. 13. Comparison of non-invariant in-plane Poisson's ratios for Configuration 1 and 2 of hexagonal lattices considering beam-level bending, axial and shear deformations. (A–C) Variation of Poisson's ratio ν_{12}, considering bending, axial and shear deformations, with the ratio of depth of cut to total thickness of cell wall, α, for different auxetic and non-auxetic configurations, for both Configuration 1 and Configuration 2. **(D–F)** Variation of Poisson's ratio ν_{21}, considering bending, axial and shear deformations, with the ratio of depth of cut to total thickness of cell wall, α, for different auxetic and non-auxetic configurations, for both Configuration 1 and Configuration 2. Note that the figure is plotted considering the geometric parameter $h/l = 1.5$.

This is partly, due to the fact that the analytical model considers the beam as being solid when the cuts are closed. However, this is not strictly the case if the cuts can slide relative to each other (if the contact is frictionless the shear transfer here would be zero). Therefore only the non-cut part is carrying shear (in the frictionless case) even if the cuts are closed. Adding friction brings finite element results closer to the solid assumption of the analysis. Fig. 6(A) depicts that the results from the two analyses match for different values of friction factors, corroborating the validity

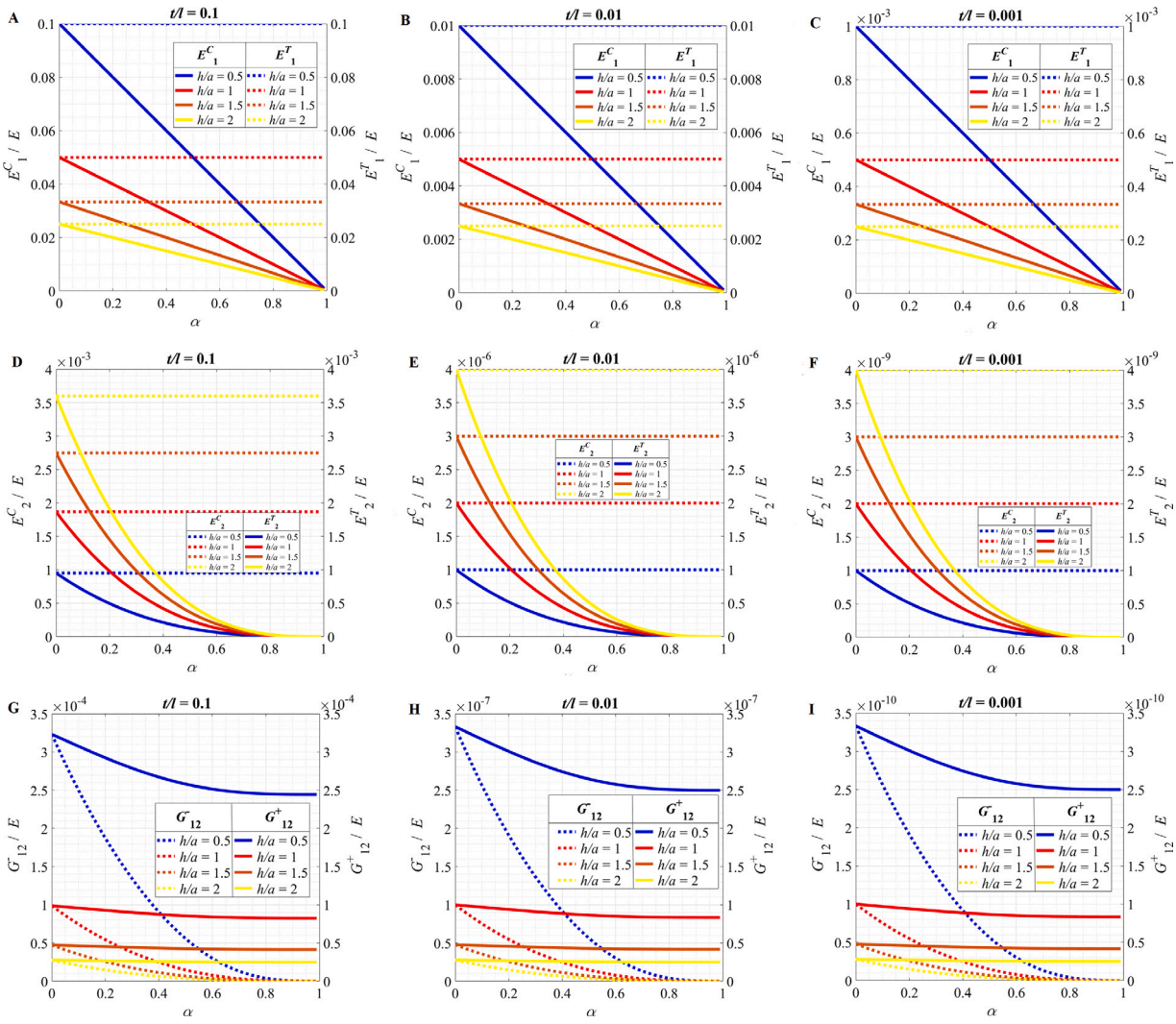

Fig. 14. Non-invariant elastic properties for rectangular lattices considering beam-level bending, axial and shear deformations. (A–C) Variation of non-dimensionalized Young's modulus in longitudinal direction, i.e., E_1/E with the ratio of depth of cut to total thickness of cell wall, α, at different values of h/a, for $t/l = 0.1, 0.01, 0.001$, considering bending, axial and shear deformations. **(D–F)** Variation of non-dimensionalized Young's modulus in transverse direction, i.e., E_2/E with the ratio of depth of cut to total thickness of cell wall, α, at different values of h/a, for $t/l = 0.1, 0.01, 0.001$, considering bending, axial and shear deformations. **(G–I)** Variation of non-dimensionalized shear modulus, i.e., G_{12}/E with the ratio of depth of cut to total thickness of cell wall, α, at different values of h/a, for $t/l = 0.1, 0.01, 0.001$, considering bending, axial and shear deformations. The Poisson's ratios come out to be zero for rectangular lattices, irrespective of the value of α. In each of the subplots, the elastic properties are presented for two opposite modes of far-field stresses considering the Configuration 1 of domain discontinuity.

of the analytical expression of deflection of a beam with cuts. Similar comparison is performed considering both bending and shear deformation in the theoretical expression (refer to Fig. 6(B)), where we find the results match more closely, since the finite element analysis factors in shear effect. This shows our beam-level theoretical model with cuts are adequately accurate for using them in the further lattice-level models. Here we note that since the expressions of lattice-level effective elastic moduli exactly converge to the closed-form expressions of established Gibson and Ashby (1999) when $\alpha = 0$, it gives an exact analytical validation of the lattice level framework. This establishes the unit call based homogenization framework, which uses beam level deformations to evaluate lattice-level effective properties, is accurate with respect to available literature. Thus, having adequate confidence in both the beam-level and lattice-level behavior, we further analyze the non-invariance in effective elastic properties of the proposed lattice materials with domain discontinuity (i.e. the introduced cuts).

Now we present the results for only bending deformation case and then for the combined case of bending, axial and shear deformation systematically. Note that the Figs. 7 to 16 are corresponding to the case of Configuration 1 for placement of domain discontinuity. The trend of non-invariance would be opposite for the Configuration 2, as discussed in Section 2.2. Fig. 7 presents the variation in effective elastic moduli of hexagonal honeycomb lattices with the ratio of the depth of cut to the total thickness of cell wall α, with applied tensile and compressive modes of far-field normal stresses (σ_1 and σ_2) along with clockwise and anticlockwise modes of far-field shear stresses (τ). Here we have considered the beam-level bending deformation only. We have considered different configurations of cell wall inclination angle θ with different values of the h/l ratio. It is important to mention here that the results are non-dimensionalized considering E_1/E, E_2/E and G_{12}/E for the elastic moduli (α is already a non-dimensional quantity). The Young's modulus of the beam members making up the lattice is denoted by E. The Poisson's ratios ν_{12} and ν_{21} are independent of α when we consider only the beam-level bending deformation, as evident from Eqs. (10) and (22) (thus the results of Poisson's ratios are not presented for this case). We can notice from the figures that for every combination of h/l ratio and inclination angle θ,

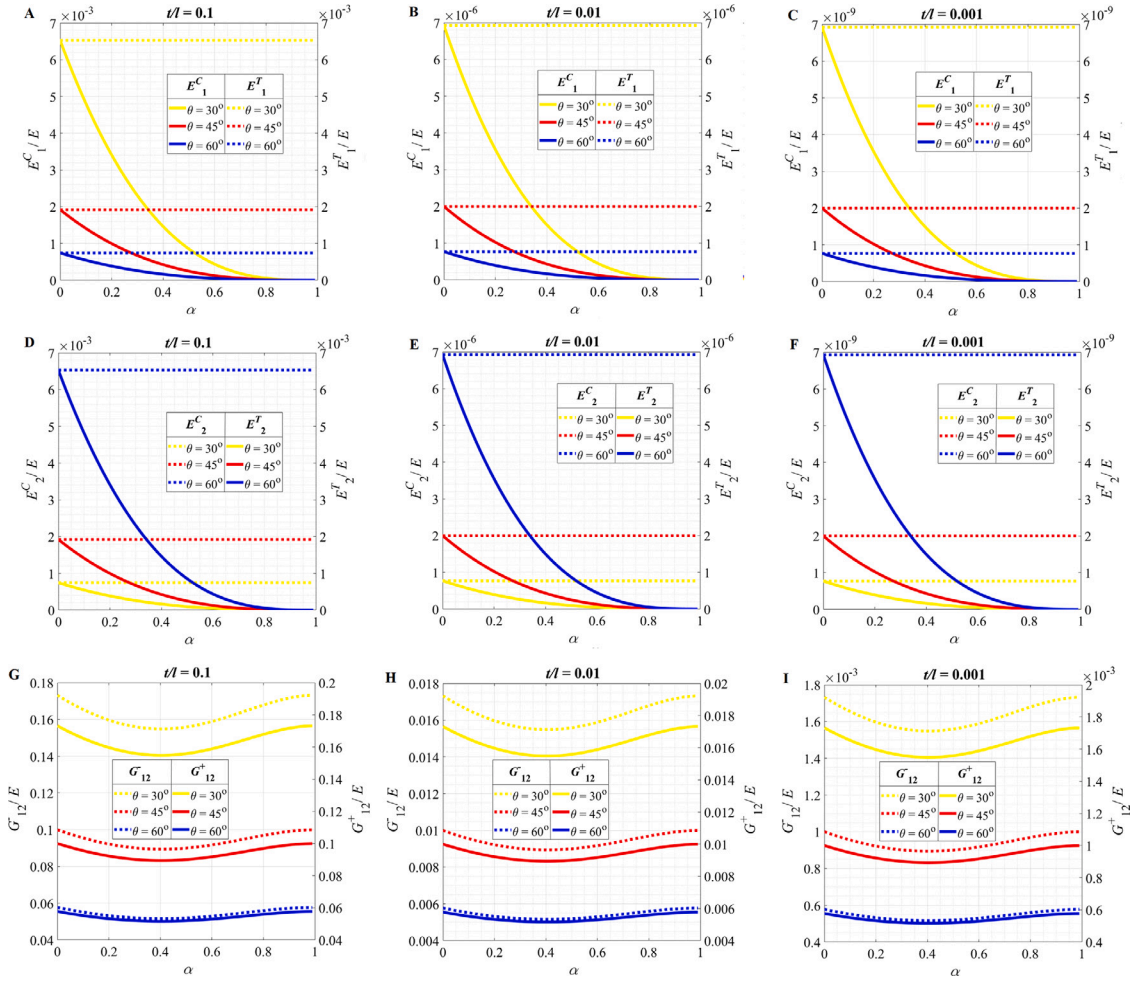

Fig. 15. Non-invariant elastic properties for rhombic lattices considering beam-level bending, axial and shear deformations. (A–C) Variation of non-dimensionalized Young's modulus in longitudinal direction, i.e., E_1/E with the ratio of depth of cut to total thickness of cell wall, α, at different values of θ, for $t/l = 0.1, 0.01, 0.001$, considering bending, axial and shear deformations. **(D–F)** Variation of non-dimensionalized Young's modulus in transverse direction, i.e., E_2/E with the ratio of depth of cut to total thickness of cell wall, α, at different values of θ, for $t/l = 0.1, 0.01, 0.001$, considering bending, axial and shear deformations. **(G–I)** Variation of non-dimensionalized shear modulus, i.e., G_{12}/E with the ratio of depth of cut to total thickness of cell wall, α, at different values of θ, for $t/l = 0.1, 0.01, 0.001$, considering bending, axial and shear deformations. In each of the subplots, the elastic properties are presented for two opposite modes of far-field stresses considering the Configuration 1 of domain discontinuity.

with an increase in the value of α, the elastic moduli decrease in the mode when the cuts open. This is because when the direction of the deflection is such that the cuts are being closed, stress due to bending moment is generated in the entire cross-section of the beam, while when the cuts are opened almost no stress is generated in those parts of the cross-section. The elastic moduli, E_1 and E_2 become independent of α, when the cuts close and thus have constant values, irrespective of the value of α (these cases are demonstrated by dashed lines in the figure corresponding to E_1 and E_2), while the shear modulus, G_{12} is dependent on α for both clockwise and anticlockwise mode of shear stress (τ). This shows that unlike in conventional materials, we can have varying elastic moduli depending on the state of stress (tension and compression modes of normal stress or clockwise or anti-clockwise modes of shear stress), where the degree of non-invariance can be programmed based on the value of α for a given microstructural configuration.

Figs. 8–11 show the variation in elastic moduli of hexagonal lattices with α, considering beam-level bending, axial and shear deformations. The applied tensile and compressive mode of normal stresses (σ_1 and σ_2) and the clockwise and anticlockwise modes of shear stresses (τ) are investigated for different unit cell geometry. Different values of t/l ratio (presenting a non-dimensional measure for the thickness of cell walls) are analyzed along with the variation of cell angle θ, considering $h/l = 1.5$. Note that the results for E_1, E_2 and G_{12} are presented here as the ratio of the elastic moduli obtained by considering bending, axial and shear deformations and the elastic moduli obtained by considering only the bending deformation. The plots in inset of Figs. 8–10 show the variation of the elastic moduli considering bending deformation with α. Thus the multiplication of the ratio of elastic modulus value presented in the main plots with the bar chart value of elastic modulus presented in the insets can lead to the actual values of elastic modulus considering bending, axial and shear deformations. We notice from the figures that for every combination of t/l and θ with an increase in the value of α, the elastic moduli increase. This increase is more evident for cases with a higher t/l ratio. As discussed in the preceding paragraph, here also the elastic moduli, E_1 and E_2 become independent of α, when the cuts close and thus have constant values, irrespective of the value of α (these cases are demonstrated by dashed lines in the figure corresponding to E_1 and E_2), while the shear modulus, G_{12} is dependent on α for both clockwise and anticlockwise mode of shear stress (τ). As the ratio t/l increases the difference in elastic moduli values in tension and compression becomes more evident. In context of the results presented in Figs. 8–10 it may be noted that we

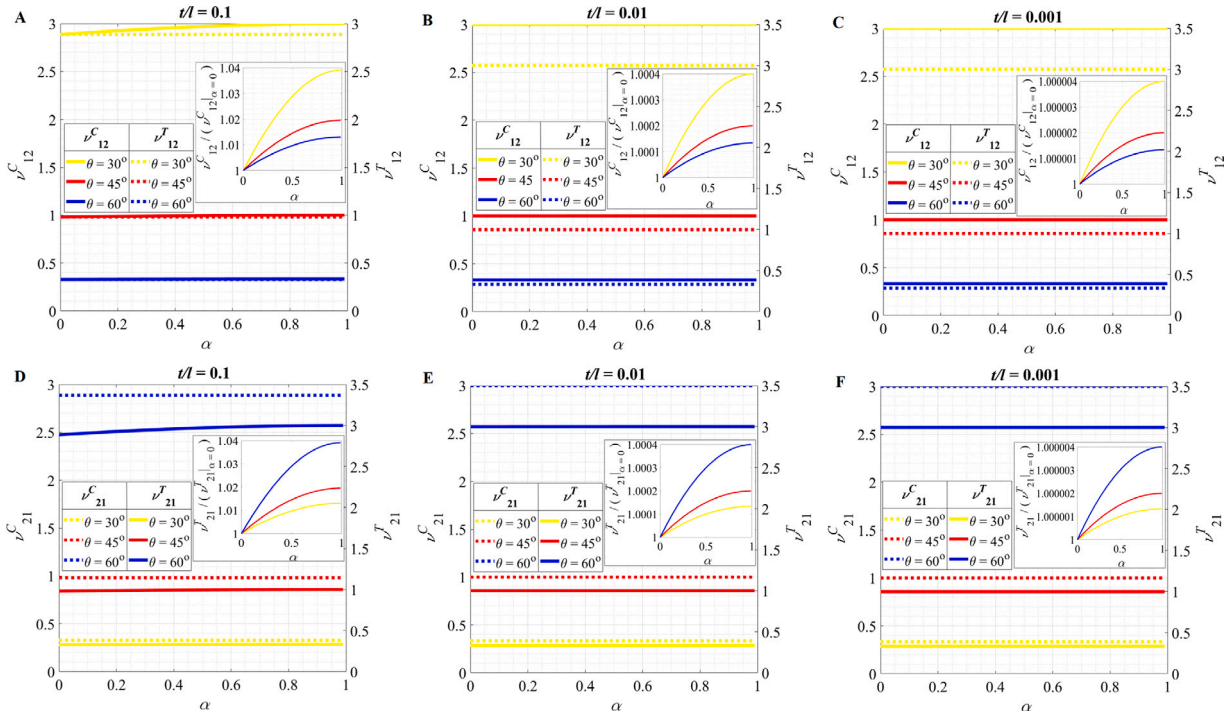

Fig. 16. Non-invariant in-plane Poisson's ratios for rhombic lattices considering beam-level bending, axial and shear deformations. (A–C) Variation of Poisson's ratio, ν_{12} with the ratio of depth of cut to total thickness of cell wall, α, at different values of θ, for $t/l = 0.1, 0.01, 0.001$, considering bending, axial and shear deformations. **(D–F)** Variation of Poisson's ratio, ν_{21} with the ratio of depth of cut to total thickness of cell wall, α, at different values of θ, for $t/l = 0.1, 0.01, 0.001$, considering bending, axial and shear deformations. The figures in inset show the variation of the ratio of Poisson's ratio, ν_{ij} at different values of α to ν_{ij} at $\alpha = 0$ $(i, j = 1, 2)$, at different values of θ. In each of the subplots, the elastic properties are presented for two opposite modes of far-field stresses considering the Configuration 1 of domain discontinuity.

have focused on the non-invariant behavior of the elastic moduli and the impact of considering beam-level bending, shear and axial deformations compared to only the beam-level bending deformation (presented here in terms of the ratios). The actual trend of variations with respect to α would be similar to that of the case considering only beam-level bending deformation, as shown in the inset plots.

Results for the Poisson's ratios ν_{12} and ν_{21} are presented considering bending, axial and shear deformations in Fig. 11. Here with an increase in α, the Poisson's ratios increase for positive cell angle θ values while they decrease for auxetic configurations. Thus the effect of α on the degree of auxeticity is evident here (unlike the case of only considering the beam-level bending deformation), wherein the degree of non-invariance can further be programmed based on the extent of domain discontinuity α.

So far we have concentrated on Configuration 1 of the proposed lattices, wherein the non-invariance in different elastic moduli with programmed domain discontinuity become apparent. Figs. 12–13 show the comparison between elastic moduli of hexagonal lattices for the two configurations (1 & 2), with α, considering beam-level bending, axial and shear deformations. The results show that the longitudinal Young's modulus E_1 and Poisson's ratio ν_{12} under compressive stress in Configuration 1 is similar to that under tensile stress in Configuration 2 while E_1 and Poisson's ratio ν_{12} under tensile stress in Configuration 1 is similar to that under compressive stress in Configuration 2. The transverse Young's modulus E_2 and Poisson's ratio ν_{21} in Configuration 1 are different to those in Configuration 2, whether under tension or compression due to the effect of change in the position of cuts in the two configurations. For the shear modulus G_{12}, the one under anticlockwise shear stress in Configuration 1 is similar to that under clockwise shear stress in Configuration 2 (and vice-versa).

Form the comparative results of Configuration 1 and 2, we note that the trend of non-invariance would be opposite under tension and compression modes of normal stresses or clockwise and anti-clockwise modes of shear stresses. For Configuration 1, we notice that for the only bending case, the expressions of the five in plane elastic properties under tensile and compressive stress are exactly opposite to that in Configuration 2. We observe that for Configuration 1, in only bending case $E_1^C \leq E_1^T$, depending on α. Similarly we get, $E_2^C \geq E_2^T$ and $G_{12}^- \leq G_{12}^+$ based on the effect of depth of cuts α, when only bending effect is taken into account. The Poisson's ratios ν_{12} and ν_{21} are similar under either compressive or tensile stress in both Configuration 1 and Configuration 2. Since in Configuration 2 for only bending case, the elastic moduli are exactly opposite to those in Configuration 1 under tensile and compressive stress and clockwise and anticlockwise shear stress, we have $E_1^C \geq E_1^T$, $E_2^C \leq E_2^T$ and $G_{12}^- \geq G_{12}^+$. For the Configuration 1, considering bending, axial and shear effect, we observe that $E_1^C \leq E_1^T$, $E_2^C \geq E_2^T$ and $G_{12}^- \leq G_{12}^+$. Also, we get $\nu_{12}^C \geq \nu_{12}^T$, $\nu_{21}^C \leq \nu_{21}^T$ in non-auxetic cases and $\nu_{12}^C \leq \nu_{12}^T$, $\nu_{21}^C \geq \nu_{21}^T$ in auxetic cases for Configuration 1. Similarly for the Configuration 2, considering bending, axial and shear effect, we observe that $E_1^C \geq E_1^T$, $E_2^C \leq E_2^T$ and $G_{12}^- \geq G_{12}^+$. Also, we get $\nu_{12}^C \leq \nu_{12}^T$, $\nu_{21}^C \geq \nu_{21}^T$ in non-auxetic cases and $\nu_{12}^C \geq \nu_{12}^T$, $\nu_{21}^C \leq \nu_{21}^T$ in auxetic cases for Configuration 2. Thus based on the placement of domain discontinuity, the tensile or compressive mode and clockwise or anticlockwise mode can have higher or lower values as per functional demands.

In this section, so far the main focus has been on the effective elastic moduli of hexagonal honeycomb lattices with non-auxetic as well as auxetic configurations (depending on the value of cell angle θ). Now the numerical investigation is extended to two other lattice forms taking into account the bending, axial and shear deformations, as proposed in Section 2.3.3 (refer to Fig. 1(C–E)). Fig. 14 shows the variation of different elastic moduli (refer Eqs. (140)–(152)) with α for different configurations of geometry in rectangular lattices. It is interesting to notice that for rectangular lattices, the Poisson's ratios become zero as given in Eqs. (142), (143), (146) and (147). For such rectangular lattices, the Young's moduli depend

significantly on α, for the case when cuts open and are independent of it when cuts are closed, while the shear modulus is dependent on α, for both clockwise and anticlockwise shear stress. Fig. 15 presents the effect of α on the effective elastic constants of rhombic cellular lattices (refer to Eqs. (153)–(162)) with different geometric configurations, considering the bending, axial and shear deformations. There is a trend of behavioral similarity in the two Young's moduli when compared with regular hexagonal honeycomb lattices, while the shear modulus can be seen to have same value for both clockwise and anticlockwise shear stress as evident from Eqs. (161) and (162). Fig. 16 presents the effect of α on the two Poisson's ratios of rhombic lattices considering the beam-level bending, axial and shear deformations. The inset figures in these plots show the variation of Poisson's ratio depending on α to the same Poisson's ratio when $\alpha = 0$. These inset figures pronounce the different values of Poisson's ratio in compressive and tensile states, which otherwise seem to be the same in the original plots. We also find that for both rectangular and rhombic lattices, as the ratio t/l increases, the elastic moduli increase.

4. Conclusions and perspective

We have proposed non-invariant lattice metamaterials through a bi-level unit cell-based framework, wherein the effective elastic moduli and Poisson's ratios can be programmed to be different in tensile and compressive normal modes or clockwise and anti-clockwise shear modes. Such behavior is not available in naturally occurring materials where the elastic moduli are normally invariant in the complementary modes of small deformation. The non-invariance is achieved here through introduction of domain discontinuity within the constituting beam elements. More interestingly, such non-invariance can be realized in the linear small deformation regime and the elastic moduli can be tailored to have higher or lower value in any mode compared to the other depending on the placement (two different configurations are proposed) and intensity of the discontinuities in a programmable paradigm.

We have derived an efficient analytical framework for the non-invariant effective elastic moduli of lattice materials taking into account the influence of domain discontinuity. First, we have presented the derivation considering only beam-level bending deformations, followed by a more generic framework involving the axial and shear deformations. The proposed analytical framework is validated extensively at the beam-level considering domain discontinuity and at the lattice level. The numerical results ascertain that the domain discontinuities, in conjunction with unit cell level geometric parameters, can impact the effective elastic constants significantly under different modes of far-field stresses. The degree of non-invariance is dependent on the severity of the introduced discontinuities, defined as a non-dimensional measure of the depth of zero-thickness (or near-zero thickness) cuts. It is further revealed that the degree of auxeticity of such lattices can be programmed to have target values (including non-invariance under different modes of deformation) as a function of the intensity and location of domain discontinuity when axial and shear deformations are included at the beam level.

Realization of the unusual non-invariant elastic moduli of bi-level architected lattice materials would lead to a range of technologically demanding niche applications where one mode of deformation requires more or less force to deform compared to the opposite mode. Besides being able to perform as a load-bearing component, the proposed metamaterial can be used as an integrated sensor for measuring the level of stress or strain in the structure. For example, under tensile far field stress, there would be more penetration of an external flux (such as luminous flux) through the metamaterial, wherein by analyzing the intensity of residual flux, the level of stress and strain can be measured in conjunction with the proposed analytical formulae.

In this work, we have concentrated primarily on hexagonal honeycomb lattices (auxetic and non-auxetic configurations) and their derivatives such as rectangular and rhombic forms. Such bending-dominated lattice forms are widely available in naturally occurring as well as engineered materials and structures. The proposed idea of achieving non-invariance on the basis of introducing domain discontinuity can be extended to other forms of lattices as well by adopting appropriate unit cells.

CRediT authorship contribution statement

P. Sinha: Carried out all the derivations, analyses and prepared the initial draft. **M.G. Walker:** Helped in finite element modeling of the beams with domain discontinuity. **T. Mukhopadhyay:** Conceived the idea, derivation, analysis, preparation of manuscript, supervision.

Declaration of competing interest

The authors declare that they have no known competing financial interests or personal relationships that could have appeared to influence the work reported in this paper.

Data availability

Data will be made available on request.

Acknowledgments

PS acknowledges the financial support from the Ministry of Education, India through a doctoral scholarship. TM would like to acknowledge the Initiation grant received from University of Southampton, United Kingdom during the period of this research work.

Appendix A. Supplementary data

Additional analytical expressions for the elastic moduli of Configuration 2.

Supplementary material related to this article can be found online at https://doi.org/10.1016/j.mechmat.2023.104691.

References

Adhikari, S., Mukhopadhyay, T., Liu, X., 2021. Broadband dynamic elastic moduli of honeycomb lattice materials: A generalized analytical approach. Mech. Mater. 157, 103796. http://dx.doi.org/10.1016/j.mechmat.2021.103796.

Anon, 2021. ANSYS academic research mechanical. In: Help System, Coupled Field Analysis Guide. ANSYS, Inc..

Cummer, S.A., Christensen, J., A., A., 2016. Controlling sound with acoustic metamaterials. Nat. Rev. Mater. 1 (3).

Dawe, D., 1984. Matrix and Finite Element Displacement Analysis of Structures. Oxford University Press, Oxford, UK.

Ding, H., Zhen, Z., Imtiaz, H., Guo, W., Zhu, H., Liu, B., 2019. Why are most 2D lattices hexagonal? The stability of 2D lattices predicted by a simple mechanics model. Extreme Mech. Lett. 32, 100507.

Dos Reis, F., Ganghoffer, J., 2012a. Construction of micropolar continua from the asymptotic homogenization of beam lattices. Comput. Struct. 112, 354–363.

Dos Reis, F., Ganghoffer, J., 2012b. Equivalent mechanical properties of auxetic lattices from discrete homogenization. Comput. Mater. Sci. 51 (1), 314–321.

Dos Reis, F., Ganghoffer, J.-F., 2014. Homogenized elastoplastic response of repetitive 2D lattice truss materials. Comput. Mater. Sci. 84, 145–155.

El Nady, K., Dos Reis, F., Ganghoffer, J., 2017. Computation of the homogenized nonlinear elastic response of 2D and 3D auxetic structures based on micropolar continuum models. Compos. Struct. 170, 271–290.

ElNady, K., Goda, I., Ganghoffer, J.-F., 2016. Computation of the effective nonlinear mechanical response of lattice materials considering geometrical nonlinearities. Comput. Mech. 58 (6), 957–979.

Fleck, N.A., Deshpande, V.S., Ashby, M.F., 2010. Micro-architectured materials: past, present and future. Proc. R. Soc. Lond. Ser. A Math. Phys. Eng. Sci. 466 (2121), 2495–2516.

Ghuku, S., Mukhopadhyay, T., 2022. Anti-curvature honeycomb lattices for mode-dependent enhancement of nonlinear elastic properties under large deformation. Int. J. Non-Linear Mech. 140, 103887.

Gibson, L., Ashby, M.F., 1999. Cellular Solids Structure and Properties. Cambridge University Press, Cambridge, UK, pp. 101–106.

Isanaka, B., Mukhopadhyay, T., Varma, R., Kushvaha, V., 2022. On exploiting machine learning for failure pattern driven strength enhancement of honeycomb lattices. Acta Mater. 239, 118226.

Karathanasopoulos, N., Dos Reis, F., Hadjidoukas, P., Ganghoffer, J.-F., 2020. LatticeMech: A discrete mechanics code to compute the effective static properties of 2D metamaterial structures. SoftwareX 11, 100446.

Karathanasopoulos, N., Dos Reis, F., Reda, H., Ganghoffer, J.-F., 2018. Computing the effective bulk and normal to shear properties of common two-dimensional architectured materials. Comput. Mater. Sci. 154, 284–294.

Karlicic, D., Cajic, M., Chatterjee, T., Adhikari, S., 2021. Wave propagation in mass embedded and pre-stressed hexagonal lattices. Compos. Struct. 256, 113087.

Kolken, H.M.A., Zadpoor, A.A., 2017. Auxetic mechanical metamaterials. RSC Adv. 7, 5111–5129.

Kundu, D., Ghuku, S., Naskar, S., Mukhopadhyay, T., 2022. Extreme specific stiffness through interactive cellular networks in bi-level micro-topology architected metamaterials. Adv. Eng. Mater..

Lai, Y., Wu, Y., Sheng, P., Zhang, Z.Q., 2011. Hybrid elastic solids. Nature Mater. 10 (8).

Li, K., Gao, X.-L., Subhash, G., 2005. Effects of cell shape and cell wall thickness variations on the elastic properties of two-dimensional cellular solids. Int. J. Solids Struct. 42 (5–6), 1777–1795.

Mousanezhad, D., Haghpanah, B., Ghosh, R., Hamouda, A.M., Nayeb-Hashemi, H., Vaziri, A., 2016. Elastic properties of chiral, anti-chiral, and hierarchical honeycombs: A simple energy-based approach. Theor. Appl. Mech. Lett. 6 (2), 81–96.

Mukhopadhyay, T., Adhikari, S., 2016a. Effective in-plane elastic properties of auxetic honeycombs with spatial irregularity. Mech. Mater. 95, 204–222.

Mukhopadhyay, T., Adhikari, S., 2016b. Free vibration analysis of sandwich panels with randomly irregular honeycomb core. J. Eng. Mech. 142 (11), 06016008.

Mukhopadhyay, T., Adhikari, S., 2017. Effective in-plane elastic moduli of quasi-random spatially irregular hexagonal lattices. Internat. J. Engrg. Sci. 119, 142–179.

Mukhopadhyay, T., Adhikari, S., Alu, A., 2019. Theoretical limits for negative elastic moduli in subacoustic lattice materials. Phys. Rev. B 99, 094108.

Mukhopadhyay, T., Kundu, D., 2022. Mixed-mode multidirectional Poisson's ratio modulation in auxetic 3D lattice metamaterials. Adv. Eng. Mater. 24 (5), 2101183.

Mukhopadhyay, T., Ma, J., Feng, H., Hou, D., Gattas, J.M., Chen, Y., You, Z., 2020a. Programmable stiffness and shape modulation in origami materials: Emergence of a distant actuation feature. Appl. Mater. Today 19, 100537.

Mukhopadhyay, T., Mahata, A., Adhikari, S., Zaeem, M.A., 2017. Effective elastic properties of two dimensional multiplanar hexagonal nano-structures. 2D Mater. 4, 029501.

Mukhopadhyay, T., Naskar, S., Adhikari, S., 2020b. Anisotropy tailoring in geometrically isotropic multi-material lattices. Extreme Mech. Lett. 40, 100934.

Mukhopadhyay, T., Naskar, S., Kundu, D., Adhikari, S., 2023. Effective elastic moduli of space-filled multi-material composite lattices. Compos. Commun. http://dx.doi.org/10.1016/j.coco.2023.101656.

Omairey, S.L., Dunning, P.D., Sriramula, S., 2019. Development of an ABAQUS plugin tool for periodic RVE homogenisation. Eng. Comput. 35 (2), 567–577.

Petyt, M., 1990. Introduction to Finite Element Vibration Analysis, Vol. 151. Cambridge University Press, Cambridge, UK, pp. 291–325.

Prajwal, P., Ghuku, S., Mukhopadhyay, T., 2022. Large-deformation mechanics of anti-curvature lattice materials for mode-dependent enhancement of non-linear shear modulus. Mech. Mater. 171, 104337.

Rahali, Y., Dos Reis, F., Ganghoffer, J.-F., 2017. Multiscale homogenization schemes for the construction of second-order grade anisotropic continuum media of architectured materials. Int. J. Multiscale Comput. Eng. 15 (1).

Singh, A., Mukhopadhyay, T., Adhikari, S., Bhattacharya, B., 2020. Voltage-dependent modulation of elastic moduli in lattice metamaterials: Emergence of a programmable state-transition capability. Int. J. Solids Struct. 40, 31–48.

Singh, A., Mukhopadhyay, T., Adhikari, S., Bhattacharya, B., 2022. Extreme on-demand contactless modulation of elastic properties in magnetostrictive lattices. Smart Mater. Struct. 31 (12), 125005.

Sinha, P., Mukhopadhyay, T., 2022. Effective elastic properties of lattice materials with intrinsic stresses. Thin-Walled Struct. 173, 108950.

Sinha, P., Mukhopadhyay, T., 2023. Programmable multi-physical mechanics of mechanical metamaterials. Mater. Sci. Eng. R 155, 100745.

Yongquiang, L., Zhiquiang, J., 2008. Free flexural vibration anlysis of symmetric rectangular honeycomb panels with scsc edge supports. Compos. Struct. 83 (2), 154–158.

Zenkert, D., 1995. An Introduction To Sandwich Construction. Engineering Materials Advisory Services., Cradley Heath, Warley, pp. 2.1–2.31.

Zhu, H., Hobdell, J., Windle, A., 2001. Effects of cell irregularity on the elastic properties of 2D voronoi honeycombs. J. Mech. Phys. Solids 49 (4), 857–870.

Zhu, H.X., Thorpe, S.M., Windle, A.H., 2006. The effect of cell irregularity on the high strain compression of 2D voronoi honeycombs. Int. J. Solids Struct. 43 (5), 1061–1078.